COMPRESSIVE AND SHEAR STRENGTHS OF FRAGMENTED ICE COVERS- A LABORATORY STUDY

by

S. T. Cheng and J. C. Tatinclaux

sponsored by

U.S. Army Corps of Engineers Cold Regions Research
and Engineering Laboratory, Hanover, N.H.
Grant No. DACA 89-76-G-057

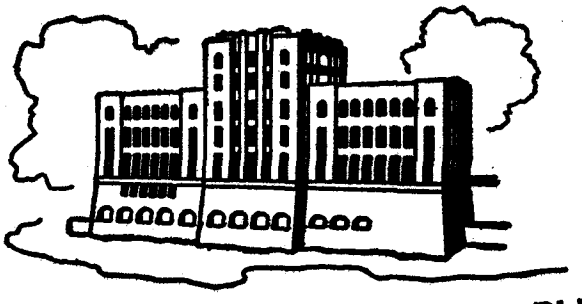

IIHR Report No. 206

Iowa Institute of Hydraulic Research
The University of Iowa
Iowa City, Iowa

August 1977

COMPRESSIVE AND SHEAR STRENGTHS OF FRAGMENTED ICE COVERS- A LABORATORY STUDY

by

S. T. Cheng and J. C. Tatinclaux

sponsored by

U.S. Army Corps of Engineers Cold Regions Research
and Engineering Laboratory, Hanover, N.H.
Grant No. DACA 89-76-G-057

IIHR Report No. 206

Iowa Institute of Hydraulic Research
The University of Iowa
Iowa City, Iowa

August 1977

ACKNOWLEDGMENTS

The following report is essentially similar to the thesis submitted by the first writer in partial fulfillment of the requirements for the degree of Master of Science in the Program of Mechanics and Hydraulics at The University of Iowa. The second writer served as thesis supervisor.

The research was supported by the U.S. Army Corps of Engineers Cold Regions Research and Engineering Laboratory, Hanover, N.H., under Grant No. DACA 89-76-G-057.

The apparatus used in the investigation were built and installed by shop personnel of the Iowa Institute of Hydraulic Research with their usual competence.

ABSTRACT

The results of an experimental study on the compressive and shear strengths of floating, fragmented ice covers are presented. The compressive strength of prestrained covers and of covers submitted to an approximately constant preload was found to be essentially equal to that of unstrained, non-preloaded covers. An important finding was that the compressive strength σ_{cr} became independent of the velocity V_c at which the load was applied when V_c became greater than 0.01 ft/sec, and that for $V_c > 0.01$ the ratio of strength to cover thickness t became, within experimental accuracy, approximately constant independent of both V_c and t. However, the difference observed between the present study and that of a previous, similar investigation led to the conclusion that small variations in the air and/or water temperatures can have a large effect on σ_{cr}, and σ_{cr}/t, probably due to their affecting the formation of cohesive bonds between the ice particles within the ice covers.

The shear strength τ of covers of various thicknesses measured in a linear and in a cylindrical apparatus were found to have essentially the same values in both apparatus. The strength τ was found to become independent of both the velocity of application of shear V_c and of the cover thickness for $V_c > 0.01$ ft/sec. The results also showed that the shear strength of covers made of crushed ice was higher than that of covers made of ice parallelepipeds, probably because of the difference in porosity and interparticular surface area between the two types of cover.

TABLE OF CONTENTS

LIST OF TABLES

LIST OF FIGURES

NOMENCLATURE

B = ice cover width

F = normal thrust on the ice cover

F_c = maximum compressive thrust of ice cover

F_r = maximum shear force

K = constant in equation $\sigma_{cr} = K V_c^{-1}$

L = ice cover length

ΔL = displacement of loading plate

g = gravitational acceleration

S = river slope

T = time

R = distance from the axis of load cell to the center of the inner rotating axle

R_c = radius of cross vane

R_r = radius of ring

R_s = radius of shear surface

t' = submerged ice cover thickness

t = ice cover thickness = $\frac{\rho}{\rho'} t'$

t_e = equilibrium ice cover thickness

V_c = acting speed, i.e. deformation rate

W = weight of ice cover

W_x = weight of ice cover along the floor slope

ρ = density of water = 1.94 slug/ft^3

ρ' = density of ice = 1.78 slug/ft^3

σ_x' = compressive strength at time T

σ_{cr} = failure compressive strength

τ' = shear stress at time T

τ = failure shear strength

τ_o = shear stress at bank-jam interface

τ_i = shear stress at the jam-water interface

θ = angular displacement

ε = strain

ε_{cr} = failure strain by compression test

ε_τ = failure strain by shearing test

I. INTRODUCTION

Ice jams can be best described as chaotic disorderly untidy affairs which at first glance appear hopelessly complex and unsuitable for analytical or even experimental studies. Problems posed by ice jams include flooding caused by blockage of channels, damage to structures, interference with navigation, and obstruction of water diversion intakes, with often large economic, physical, and even human losses as consequences. Attempts have been made, out of necessity, to understand and predict the conditions under which ice jams will form, their evolution in thickness and profile, the forces that they may exert on existing structures (bridge piers, dams, etc...) or structures specially built for their control (ice booms). Ice-jam understanding calls upon the knowledge of hydraulics to predict the added resistance to flow, resulting backwater curves in channel and flooding potential; as well as upon mechanics of materials for determination of jam mechanical properties, compressive and shear strengths either as consolidated ice covers once the individual ice floes composing the jam are frozen together to form a solid ice cover, or as unconsolidated aggregates of ice floes of various dimensions, from a few feet to several tens of feet in lateral dimension and from a few inches to a few feet in thickness. The actual problem of ice-jam mechanics is further complicated when frazil ice accumulates below a jam originally formed of large ice floes. Detailed description of ice jams and reviews of the literature related to their mechanics have been given by Bolsegna (1968) and Uzuner and Kennedy (1974). Histories of specific jams have been published by the U.S. Army Corps of Engineers (1967), by Frankenstein and Assur (1972), and by others.

When an ice jam is considered to be a continuous medium, a first approximation to a most complicated natural phenomenon, the forces acting on a control volume of length dx and width B (channel width), as depicted in Figure 1, are

F = the normal thrust per unit width on the upstream face of the control volume.

F+dF = the normal thrust on the downstream face.

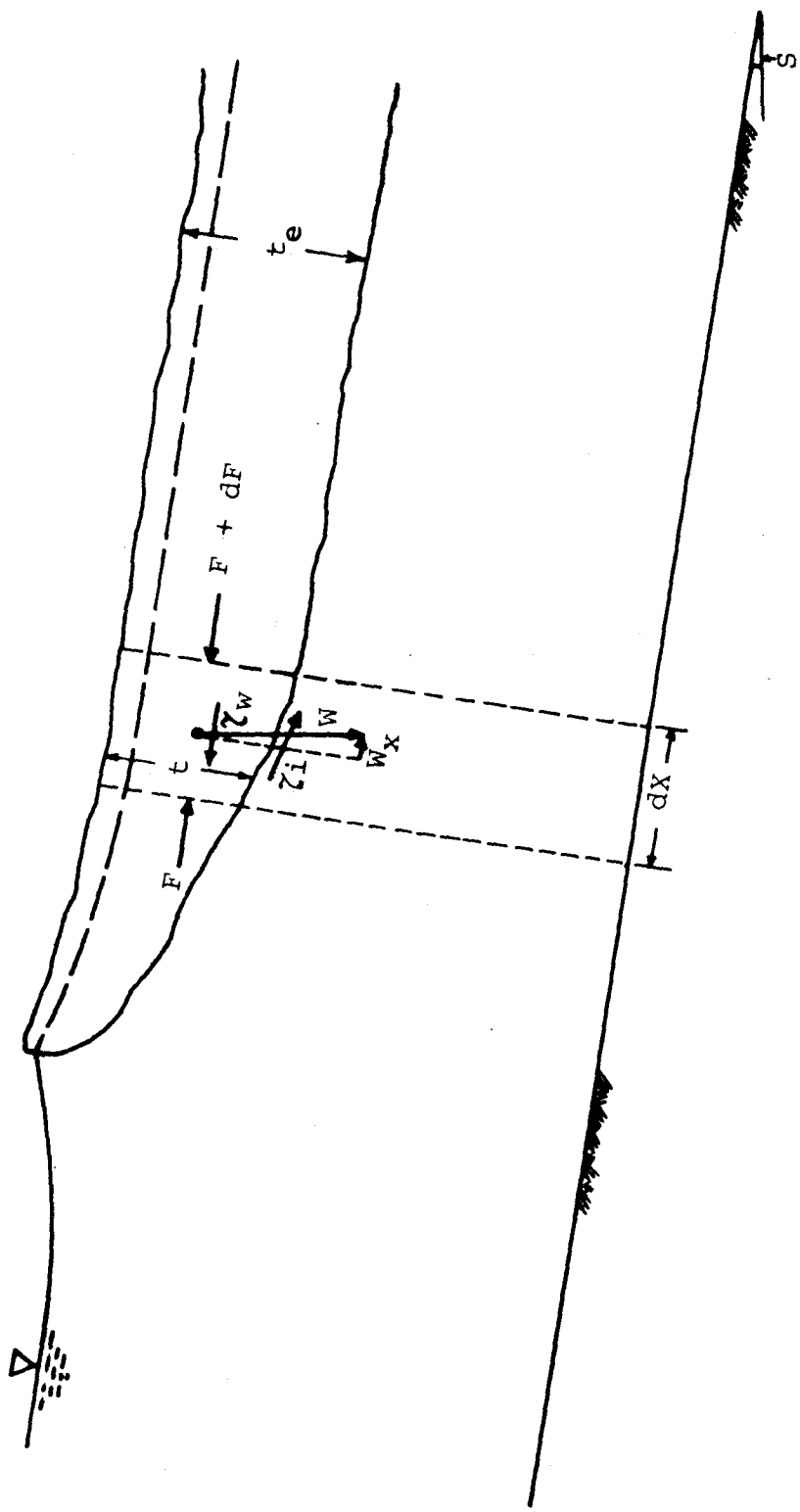

Figure 1 Definition sketch.

$t\tau\ dx$ = the shear force at the bank-jam interface

$B\tau_i dx$ = the shear force at the jam-water interface due to the flowing water beneath the jam.

$W_w = \rho' g\ t\ B\ dx\ S$ = component of jam weight in flow direction

The force balance equation of the control volume is

$$\frac{d\ F}{d\ x} + 2\ t\tau = B\tau_i + \rho'\ g\ t\ B\ S \qquad (1)$$

In the available mathematical models for ice-jam equilibrium, by Pariset et al (1966) and by Uzuner and Kennedy (1974, 1976), the equilibrium thickness t_e of the jam is determined by the condition

$F = F_c$ = maximum compressive strength of cover of thickness t_e

or

$$\left.\frac{dF}{dx}\right|_{t=t_e} = 0$$

The force exerted by the jam on any structure will then be equal to F_c. Assuming that the jam has uniform properties across the channel width, then

$$F_c = \sigma_c\ B\ t_e$$

where σ_c is the compressive strength of a fragmented cover of thickness t_e.

As can be seen from (1) the shear strength τ of the cover plays an important role in the jam thickness. At the limit $\tau = 0$, the equilibrium condition can never be reached, and the jam thickens continuously at the same time that it progresses upstream.

Uzuner and Kennedy (1974) describe the development of a jam as follows:

> "As the length of the jam is increased by the arrest of the newly arrived floes near its upstream end, the total streamwise external force applied to the jam upstream from any section will cause the jam to thicken by failure or "collapse" of the ice cover, until its shear and compressive strength are great enough to balance the applied forces,... Moreover, the failure results from displacement between fragments, and not in general from rupture of the pieces of ice." (page 12)

In past years, experimental investigations of the relationship between the failure compressive strength σ_{cr} and shear strength τ of fragmented ice cover and ice cover thickness and deformation rate were conducted in the IIHR Low Temperature Facility. In their studies of σ_{cr} Uzuner (1974) and Nakato (results reported by Tatinclaux et al. (1976)) found that σ_{cr} the failure compressive strength is inversely proportional to deformation rate.

The investigation reported herein was the continuation of these previous studies on σ_{cr} and τ. The objects of this study were threefold: First, to investigate the relationship between σ_{cr} and t. Second, to see whether σ_{cr} is affected by preloading the fragmented ice cover. Third, to determine whether there is a significant difference in τ between the results obtained in Merino's (1974) investigation and this investigation in which two kinds of shearing test apparatus, rectangular and cylindrical, were used.

The experimental procedures, techniques and results of compressive strength and shear strength tests are described and presented in Sections II and III, respectively. Discussion of the results and a summary of the conclusions observed from the study are given in Section IV.

II. COMPRESSIVE STRENGTH OF FRAGMENTED ICE COVERS

A. Introductory Remarks. In the tests reported by Uzuner and Kennedy (1974) for the determination of the compressive strength σ_{cr} of fragmented ice covers, it was found that the ice covers tested were too long and, thus, that the part of the cover far away from the area of application of the compressive force did not become stressed during loading. Instead, the load applied was transferred through shear to the walls of the tank, and consequently the observed failures might have been caused partly by shear. Furthermore, a buckling type of failure was observed to occur at times, which was believed to be an artifact of the laboratory test apparatus and not likely to happen in most field situations. In Nakato's tests reported by Tatinclaux et al (1976), shorter cover of lengths 3.6 ft, 3.0 ft, 2.6 ft and 2.0 ft, were used. It was observed that the compressive strength of the ice cover was then independent of the cover length L. Therefore, in the

present experiments, just one cover length, 2 ft, was tested.

B. Experimental Unit. The compressive strength experiments were conducted in the 2-ft deep, 3-ft wide, and 19-ft long insulated force tank of the IIHR Low Temperature Flow Facility. The compressive apparatus, shown schematically in Figure 2, consisted of three main parts.

1. Force-driving mechanism. The normal force applied to the fragmented ice cover was created by a driving plate attached to the motorized carriage supported by four ball-bushings riding on 1-inch diameter rails. The carriage was driven by a variable speed, one-horsepower DC motor on two tracks which were affixed to the tops of the long walls of the tank. The motor speed was remotely controlled through a SCR drive control, and the carriage speed could be adjusted through a dial setting on the SCR drive control regulator. The range of carriage speed could be varied from 0.004 cm/sec to 2.4 cm/sec. The relationship between carriage speed and dial setting was determined by direct measurement of carriage speed for a series of dial readings. The speed of the carriage could also be inferred during each experiment from the output of the displacement measuring potentiometer described later.

2. Force measuring system. The driving plate was attached to the carriage through a moment insensitive dynamometer shown in Figure 3. A Statham Universal transducing cell, Model UC3, and load cell, Model UL4, were connected to the dynamometer and used to measure the compressive force applied by the driving plate on the fragmented ice cover. Two load cells, of capacity up to 200 lb and 500 lb, were used depending on the expected magnitude of the compressive force. The voltage output of the transducer was amplified by and recorded on a multiple channel recorder Beckman Dynograph R Type. A block diagram of the transducer circuit is shown as Figure 4. The force measuring system was calibrated by applying known horizontal loads to the driving plate. The calibration curve was found to be linear between load and output voltage, with calibration constants as listed in Table 1.

3. Displacement measuring system. The displacement of the driving plate was measured by a 10-turn potentiometer, shown on Figure 5, attached to the carriage. A rubber wheel at the end of the potentiometer shaft was set in contact with one of the two racks installed on the walls of the tank and rotated while the carriage moved. The voltage output of the potentiometer was

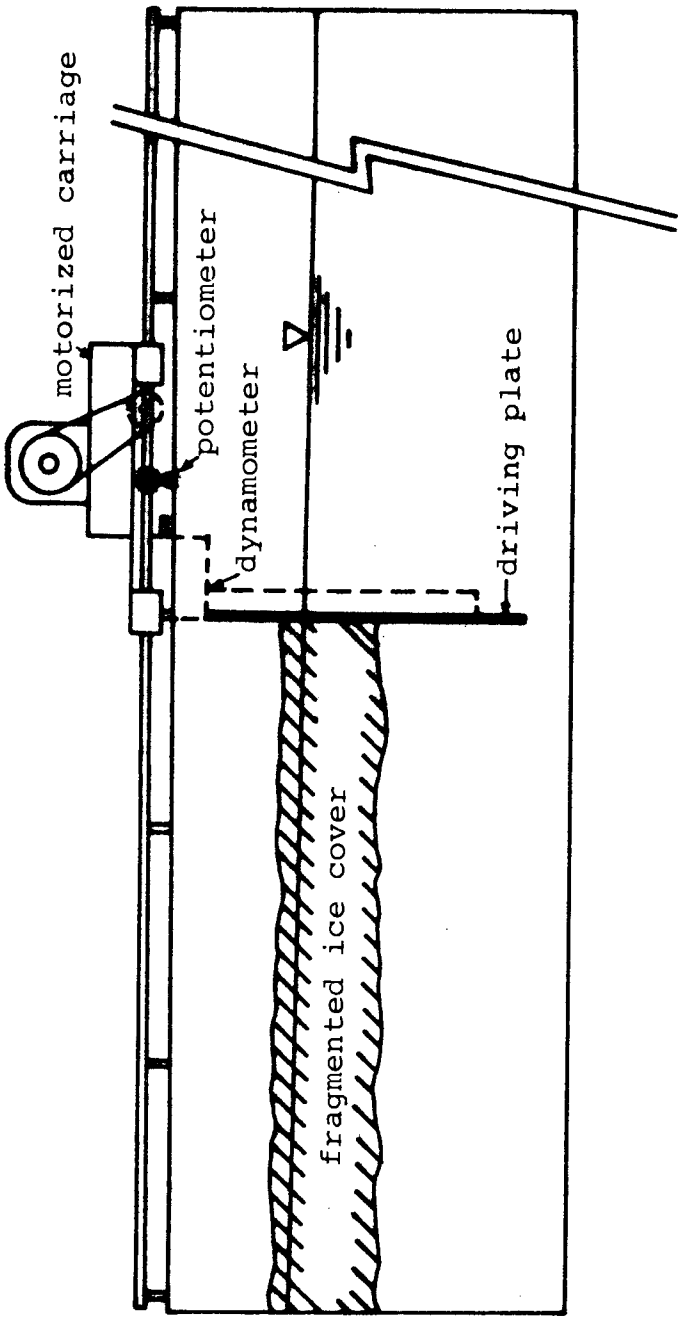

Figure 2 Schematic rendering of apparatus used in compressive strength tests.

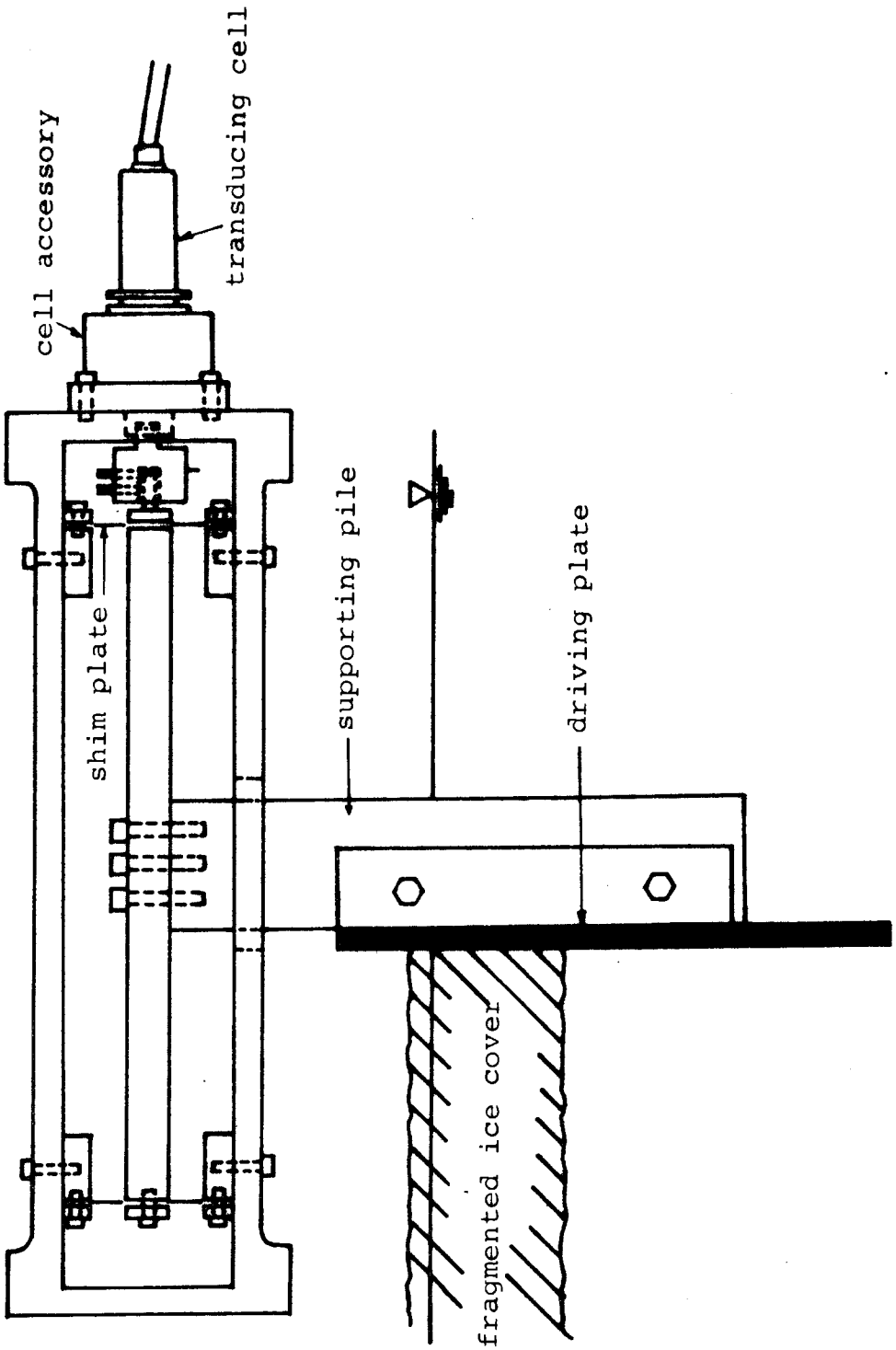

Figure 3. Dynamometer.

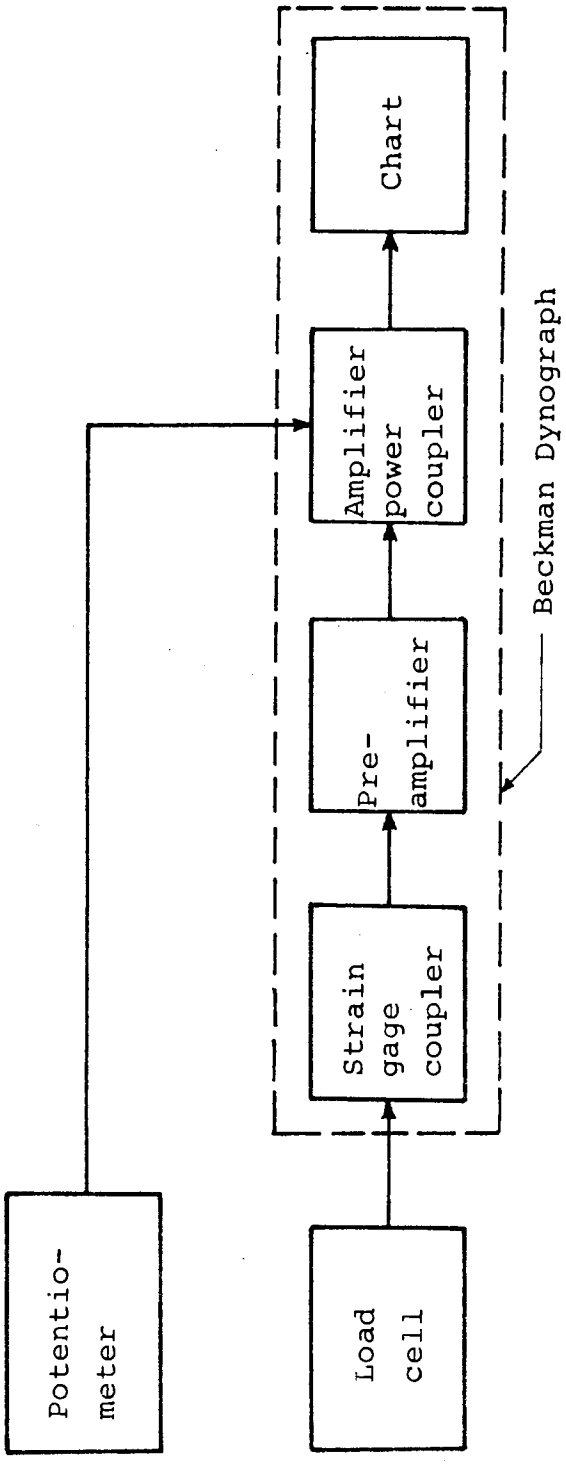

Figure 4. Force-displacement transducer circuit block diagram.

Table 1 Calibration ratios of force to output voltage for load cells with different capacities. (unit: lb/mv).

Sensitivity / Load Cell	0.5 mv/cm	1.0 mv/cm	2.0 mv/cm	5.0 mv/cm
500 #	37.34	38.31	39.45	38.70
200 #	---	14.79	14.90	14.84

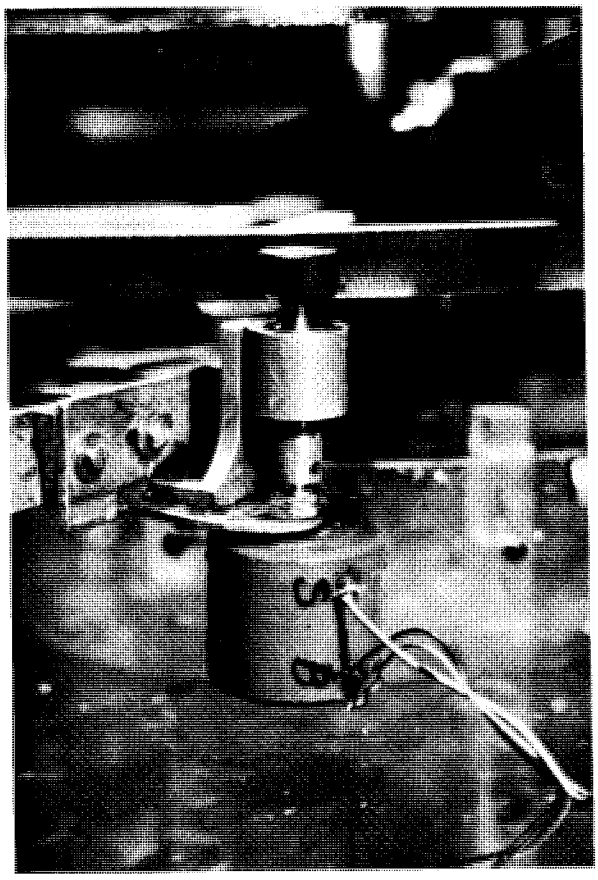

Figure 5. Photograph of potentiometer (mounted on cylindrical shear apparatus)

also amplified by and recorded on a second channel of the Beckman Dynograph. The calibration constant was found to be 0.011 cm/mv for a recorder sensitivity of 200 mv/cm. The block diagram of the transducing circuit is also shown in Figure 4.

C. Test Material. The fragmented ice covers tested were made of ice parallelepipeds of dimension, $1\frac{1}{2}$ inch x $1\frac{1}{4}$ inch x $\frac{5}{16}$ inch, manufactured in a commercial ice-maker.

D. Experimental Set-up and Procedure.

1. Experimental Set-up. During all experiments the room temperature was kept nearly constant at 0°C. Prechilled water was pumped into the tank and allowed to reach a uniform temperature nearly equal to 0°C. The required quantity of ice to give the desired cover thickness and cover length (L = 2.0 ft.) was placed in front of the driving plate. The floating ice cover was gently agitated with a rod to insure as uniform a cover thickness as possible. Measurement of the floating ice cover thickness was performed by means of an L-shape staff gage fitted with an inch scale and attached with a 3 inch x 5 inch horizontal rectangular plate. The staff gage was inserted through the ice cover and raised until the plate came in contact with the bottom of the cover. The thickness of the cover was read from the scale on the gage staff. The thickness was measured at four or more points of the cover in order to verify that the cover thickness was practically uniform.

The Beckman recorder was turned on and allowed to warm up at the beginning of each series of experiments. The initial output voltages of the load cell for zero applied load and of the potentiometer for zero displacement were balanced to give zero output voltage by adjusting the balancing circuit of the Dynograph recorder strain gage coupler. Then the heat pens of the recorder were set to zero position on the recording chart. The SCR drive control dial was set at the position corresponding to the desired carriage velocity and the carriage was set in motion. The force and displacement outputs were recorded versus time on the dynograph chart.

2. Conduct of experiments. In order to determine the influence, if any, of preload on the compressive strength of floating, fragmented ice covers, several series of test were performed. A first series of "ordinary"

tests was run where the motion of the carriage; i.e. of the driving plate, was stopped only after failure of the ice cover had occurred. The test procedure was identical to that followed in the experiments by Uzuner (1974) and by Nakato (reported by Tatinclaux et al (1976)). In a second series of experiments, the motion of the plate was halted when the load registered by the load cell had reached a value equal to a prescribed percentage of the failure load obtained in the first series of experiments for the same nominal experimental condition of cover thickness and carriage speed. After a waiting period of five minutes, the carriage was reset in motion at the initial speed until failure of the cover occurred. A typical example of the overall force record obtained in this manner is given in Figure 6.

However, as can be seen in Figure 6, as soon as the plate motion was first halted, the force registered by the load cell started to decrease; indicating relaxation of the ice cover. In these experiments the ice covers were in fact subjected to an initial prestrain rather than to a constant preload. A third series of experiments was then undertaken. In these latter runs, the carriage was set into motion until the load applied to the cover reached a prescribed value, called initial preload, at which point the carriage was stopped. It was restarted as soon as the actual load registered by the load cell had dropped to approximately 70% to 80% of the initial preload, and immediately stopped again, since the registered load was observed to increase at once back to the value of the initial preload. This stop and go procedure (an exercise in digital dexterity) was continued for five minutes, after which the driving plate was set in continuous motion at the initial speed until the cover failed. An example of force-versus-time record obtained under this procedure is shown in Figure 7. This procedure was expected to yield more realistic values of the compressive strength of an ice cover under constant preload. As previously reported by Uzuner (1974) and Nakato (1976), considerable variation in the failure force was observed from one test to another for identical nominal experimental conditions. Therefore, experiments were run an average of 8 times under the same nominal conditions. In addition, the ice samples were changed after a few runs since they were observed to wear, chip, melt slightly or otherwise change their geometric characteristics which could further cloud comparisons between results obtained under different conditions of cover thickness and carriage speed.

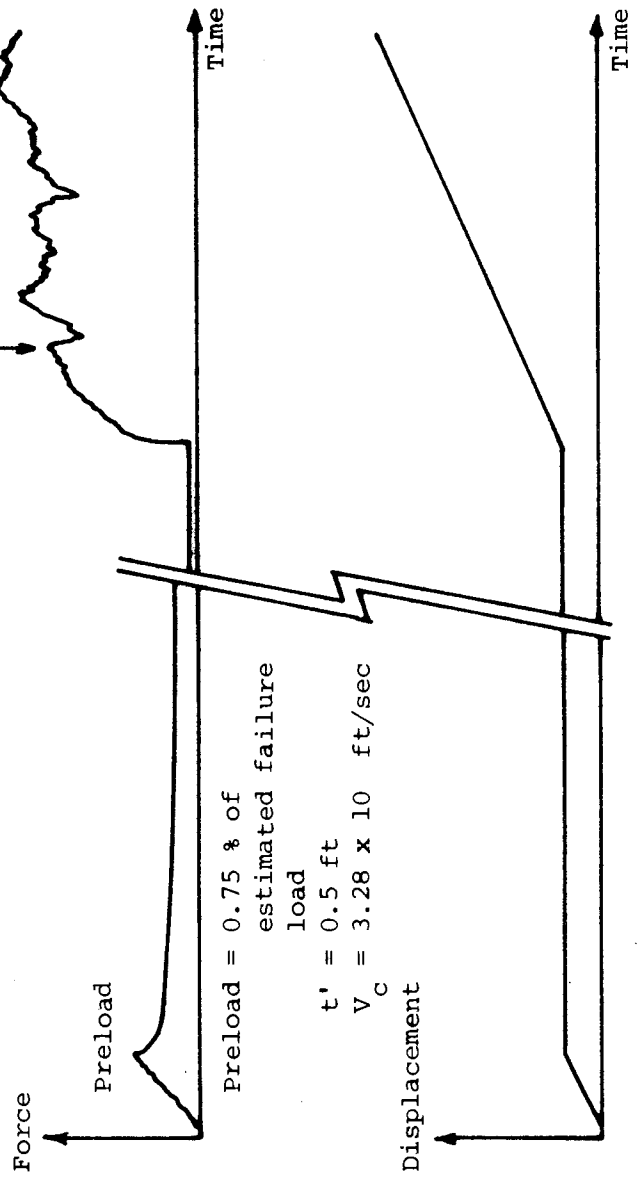

Figure 6. Typical example of force-displacement-time record for compression test with preload applied once

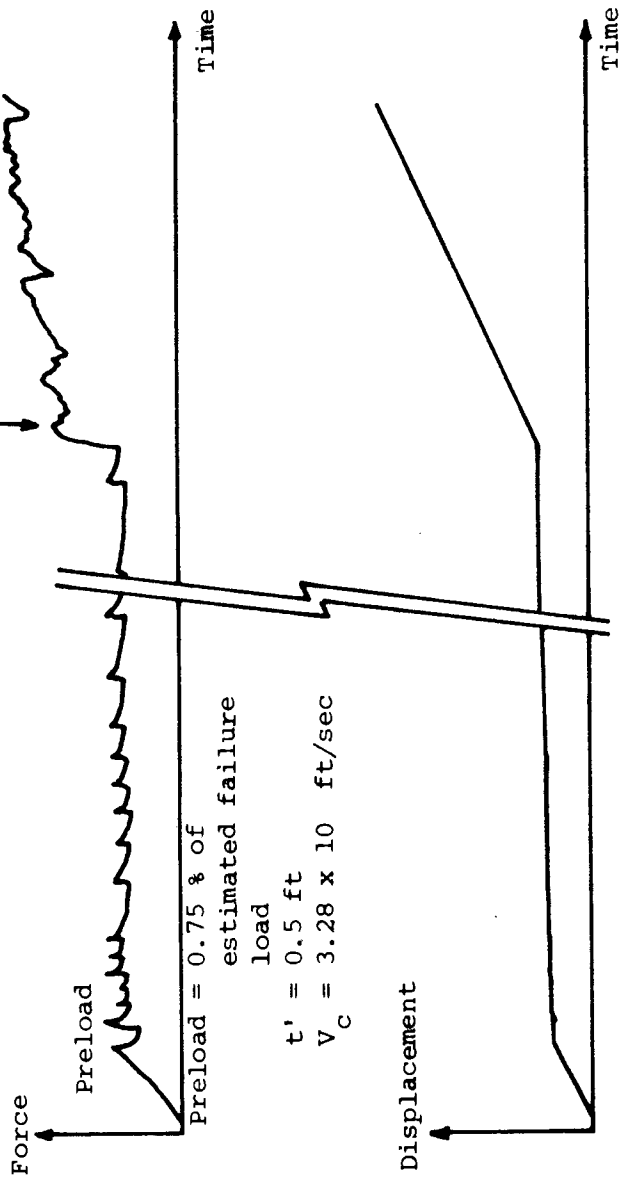

Figure 7. Typical example of force-displacement-time record for compression test with preload kept approximately constant

E. Discussion of Experimental Results

1. Compression of tests without preloading. Typical experimental force-displacement-time records are shown in Figure 8. The force exerted on the driving plate by the fragmented ice cover is given by the upper trace and the displacement of the driving plate is given by the lower trace. The time scale is indicated on the upper edge of the record.

During the compression process, the ice floes rearranged themselves continuously in the ice cover and the porosity of the ice cover decreased, increasing the interparticle contact between ice floes and, consequently, the resistance to the driving plate increased until it reached a maximum value then dropped either abruptly or gradually depending on the velocity V_c of the driving plate; i.e. on the deformation rate of the fragmented ice cover. This drop in the registered force indicated failure of the ice cover, and the maximum force recorded was taken as the failure force of the cover. Three different types of failure were observed during the compression tests. For the lower deformation rates, $V_c \sim 0.001$ ft/sec, (case 1 in Figure 8), the fragmented ice cover was not actually fractured; instead, interparticle bonding occurred leading to a buckling type of failure at some point between the driving plate and the end of the tank. The force decreased slowly after reaching a maximum value which was taken as the failure strength of the ice cover.

In the middle range of deformation rates, $0.001 \text{ ft/sec} < V_c < 0.006$ ft/sec, (case 2 and case 3 in Figure 8), cracks were observed to form in the ice covers, most of which failed by sudden collapse evidenced by an abrupt drop in the recorded force. The maximum force before collapse was taken as the failure strength. When the compression process was continued further, the force started to increase again until a second peak appeared. This indicated that the individual ice floes in the fragmented ice cover had rearranged themselves and that the cover had recovered at least part of its strength. Finally, for higher deformation rates, $V_c > 0.006$ ft/sec, (case 4 in Figure 8), the fragmented ice cover was found to fail usually successively by fracture near the driving plate. The force in the record fluctuated over a small range after it had arrived at some maximum value.

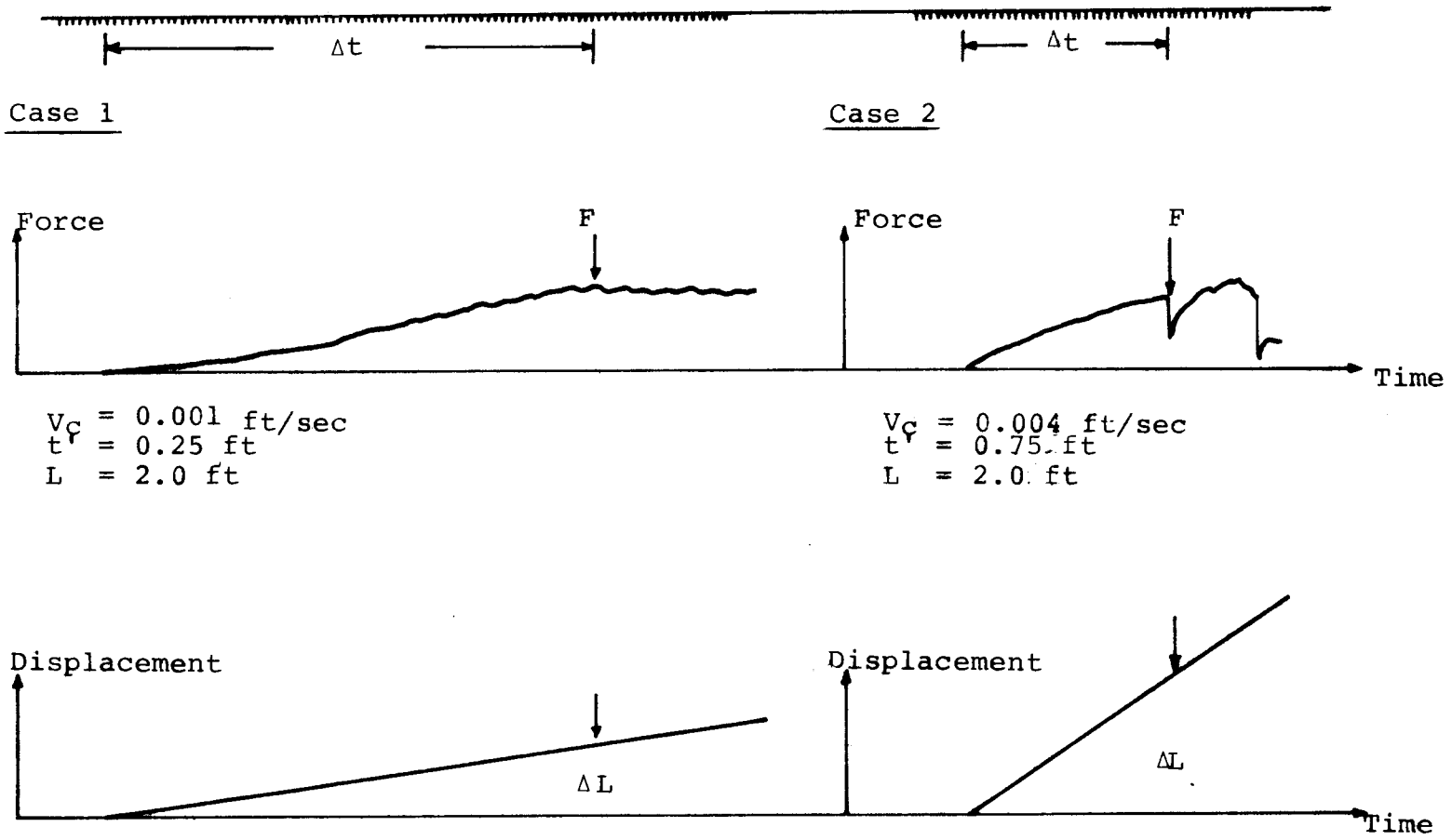

Figure 8. Typical examples of force-displacement-time record for compression tests without preloading.

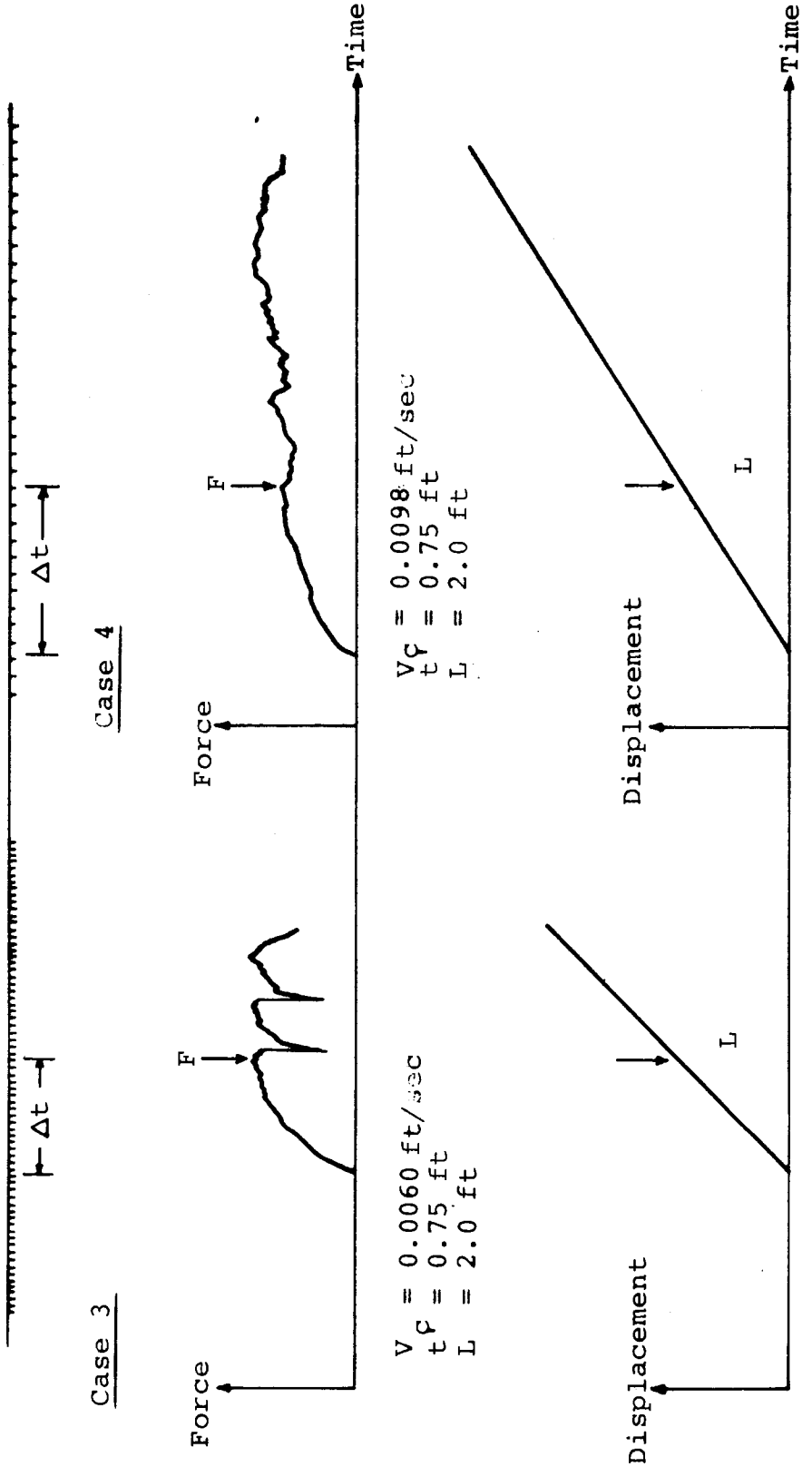

Figure 8. (continued)

The first maximum force was taken as the failure strength, but could not be as well defined as for the lower and middle range of deformation rates.

On the records, the carriage displacement-versus-time curve was usually a straight line indicating that the driving plate moved at a constant speed and that the fragmented ice cover was compressed under constant deformation rate. However, due to the mechanism of the carriage system, the speed of the driving plate could not be kept at a constant rate when the exerted force exceeded 300 lb, as shown in Figure 9. All the experiments were under this limitation. The displacement at failure, ΔL, was measured as well as the time, T, from the beginning of the experiment to the occurrence of failure.

2. Compression tests with preloading. As mentioned previously, Figures 6 and 7 show that when the preload was applied once (prestrained ice cover), the force registered by the load cell decreased as soon as the driving plate stopped, rapidly at first, then at a slower rate. When the driving plate was restarted after a lapse of time of 5 minutes, the force rose instantly back to practically the initial level of preload and then increased almost linearly with displacement until failure happened. This phenomenon is tentatively explained by the effect of melting and refreezing at the ice particle interfaces, with the accompanying production of cohesive welds, under the application of pressure on fragmented ice blocks. This formation of cohesive welds also required time as well as the applied pressure. Accordingly, the 5-minute long prestrain allowed the time and provided the pressure for the cohesive welds to form. As a result, the fragmented ice cover became a temporarily rigid cover which gave a quick responsive resistance force to the restarting driving plate. When the new force applied to the temporarily rigid ice cover exceeded the amount of preload, the cohesive welds melted and the ice particles continued to rearrange themselves with, as a result, an increase in the interparticle contact surface and hence in the strength until failure occurred.

However, the force diagram of the compressive test with preload being kept approximately constant is somewhat different from that of the compression test with preload applied once. In the former case, failure of the ice cover happened almost immediately after restarting the driving plate. A suitable and reasonable explanation for this phenomenon is not known; but, it is likely to be due to the frequent application of impact

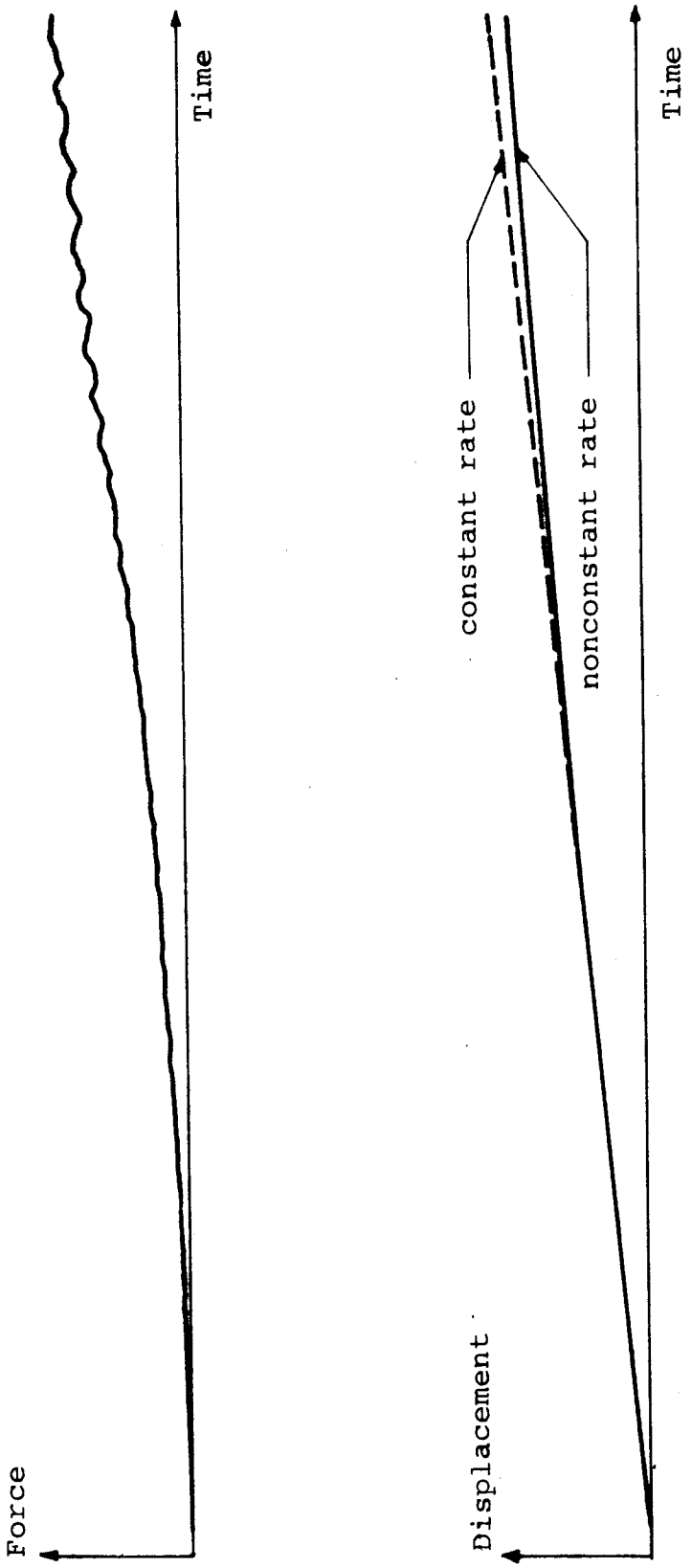

Figure 9. Force-displacement-time record for compressive load greater than 300 lbs.

onto the ice cover during the 5-minute preloading.

F. Data Calculation and Listing. The average compressive strength, σ_{cr}, of the ice cover was defined as

$$\sigma_{cr} = \frac{\frac{1}{n}\sum_{i=1}^{n} F_i}{B\ t} \tag{1}$$

where

n = the number of runs performed under nominally identical conditions

F_i = failure force recorded in the i-th run.

B = width of the ice cover (3.0 ft).

t = ice cover thickness in each set of runs.

The ice cover thickness, t, is defined as

$$t = \frac{\rho}{\rho'} t'$$

where

ρ = density of the water at 0°C.

ρ' = density of the ice at 0°C.

t' = average submerged ice cover thickness.

The average deformation rate, V_c, of fragmented ice cover was defined as:

$$V_c = \frac{1}{n}\sum_{i=1}^{n} \frac{\Delta L_i}{\Delta t_i} \tag{2}$$

where

ΔL_i = displacement of driving plate when ice cover failed in the i-th run.

Δt_i = time elapsed when ice cover failed (i-th run)

The average strain at failure, ε_{cr}, of the fragmented ice cover was defined as:

$$\varepsilon_{cr} = \frac{\sum_{i=1}^{n} \Delta L_i}{n\ L} \tag{3}$$

where

L = ice cover length (L = 2 ft)

Using the above definitions and the data collected from the records, the results of the compression tests without preloading and with preloading

(both applied once and kept approximately constant) are listed in Tables 2 and 3, respectively.

G. Graphical Presentation of the Results.

1. Experiments without preloading.

(a) Stress-strain relationship. From the force-displacement-time records, the longitudinal normal stress, σ_x', experienced by the ice cover at any time T, and the corresponding strain, ε, defined as $\Delta L/L$, where $\Delta L = V_c T$ is the distance traveled by the driving plate at time T, could be determined. Typical stress-strain curves are shown in Figures 10, 11, and 12 for submerged ice cover thickness of 0.25, 0.50, and 0.75 ft, respectively.

In each figure, the data were plotted for different speeds of driving plate, i.e. of strain rate, the ice cover length and thickness being held constant. It can be seen that the stress σ_x' increased concave upward under the lower rates of deformation and convex upward under the higher rates of deformation. Furthermore, the yield compressive strength σ_{cr}, decreases with increasing speed, V_c, of driving plate and thus with rate of deformation. This phenomenon is attributed to freezing of the liquid film between the contact surfaces of the particles, thus forming a natural weld that produces a cohesive bond between the ice-particle surfaces. Since lower deformation rate allows more time for freezing and thus for cohesive bonds to develop, the compressive strength of the fragmented ice cover should increase with decreasing rates of deformation. A yet unclear phenomenon exhibited by the results is the variation of yield strain ε_{cr} with acting speed V_c as shown in Figure 13. It can be seen that ε_{cr} increases practically linearly with increasing V_c for the two values of cover thicknesses of 0.5 ft and 0.75 ft, while ε_{cr} decreases nonlinearly with increasing V_c when t' was equal to 0.25 ft, as was already observed in Nakato's experiments reported by Tatinclaux et al (1976), in which the strain at the yield point always decreased with increasing rates of deformation. The only tentative explanation which appears reasonable at this time for this increase or decrease tendency of ε_{cr} with increasing V_c is to be sought in the effect of the ratio L/t' of cover length to cover thickness on the type of failure the cover undergoes: possible buckling for thin cover as opposed to "crushing" for thicker cover. This possible

Table 2. Summary of experimental results from compression tests without preloading

No.	t' (ft)	F (lb)	σ_{cr} (lb/ft^2)	σ_{cr}/L (lb/ft^3)	ϵ_{cr} (%)	$V_c \times 10^{-3}$ (ft/sec)
c-1	0.25	86.65	106.31	425.00	7.36	0.51
c-2	0.25	17.07	20.94	83.76	3.75	0.93
c-3	0.25	20.33	24.94	99.76	3.72	1.14
c-4	0.25	12.18	14.95	59.80	2.24	1.20
c-5	0.25	10.43	12.79	51.16	1.41	2.15
c-6	0.25	5.72	7.02	28.08	0.98	3.21
c-7	0.25	4.20	5.15	20.60	0.70	4.34
c-8	0.50	32.85	20.15	40.30	1.91	2.14
c-9	0.50	21.31	13.07	26.14	2.08	3.42
c-10	0.50	17.70	10.86	21.72	2.79	4.74
c-11	0.50	10.60	6.50	13.00	3.07	7.63
c-12	0.75	83.41	34.11	68.22	4.19	2.82
c-13	0.75	65.46	26.77	53.54	4.48	4.22
c-14	0.75	41.03	16.78	33.56	4.84	6.00
c-15	0.75	35.09	14.35	28.70	5.72	9.21

Table 3. Summary of experimental results from compression tests with preloading

No.	t' (ft)	Preload (%)	F (lb)	σ_{cr} (lb/ft^2)	$V_c \times 10^{-3}$ (ft/sec)
PA1	0.50	25	23.36	14.33	3.2
PA2	0.50	50	20.31	12.46	3.5
PA3	0.50	75	27.19	16.68	3.0
PA4	0.50	25	18.67	11.45	4.8
PA5	0.50	50	16.66	10.22	5.0
PA6	0.50	75	16.35	10.03	4.7
PA7	0.50	25	15.11	9.27	6.4
PA8	0.50	50	16.06	9.85	6.4
PA9	0.50	75	15.27	9.37	6.3
PA10	0.75	25	64.11	26.22	5.1
PA11	0.75	50	70.13	28.68	4.4
PA12	0.75	75	76.85	31.43	4.5
PA13	0.75	50	63.58	26.00	6.1
PA14	0.75	75	60.25	24.64	6.7
PB1	0.50	50	22.29	14.86	3.2
PB2	0.50	75	25.47	16.98	3.1
PB3	0.50	50	14.39	9.59	4.9
PB4	0.50	75	17.18	11.45	5.1
PB5	0.50	50	9.90	6.60	7.0
PB6	0.50	75	12.90	8.60	7.0

P.S. * PA preload applied once
* PB preload applied approximately constant

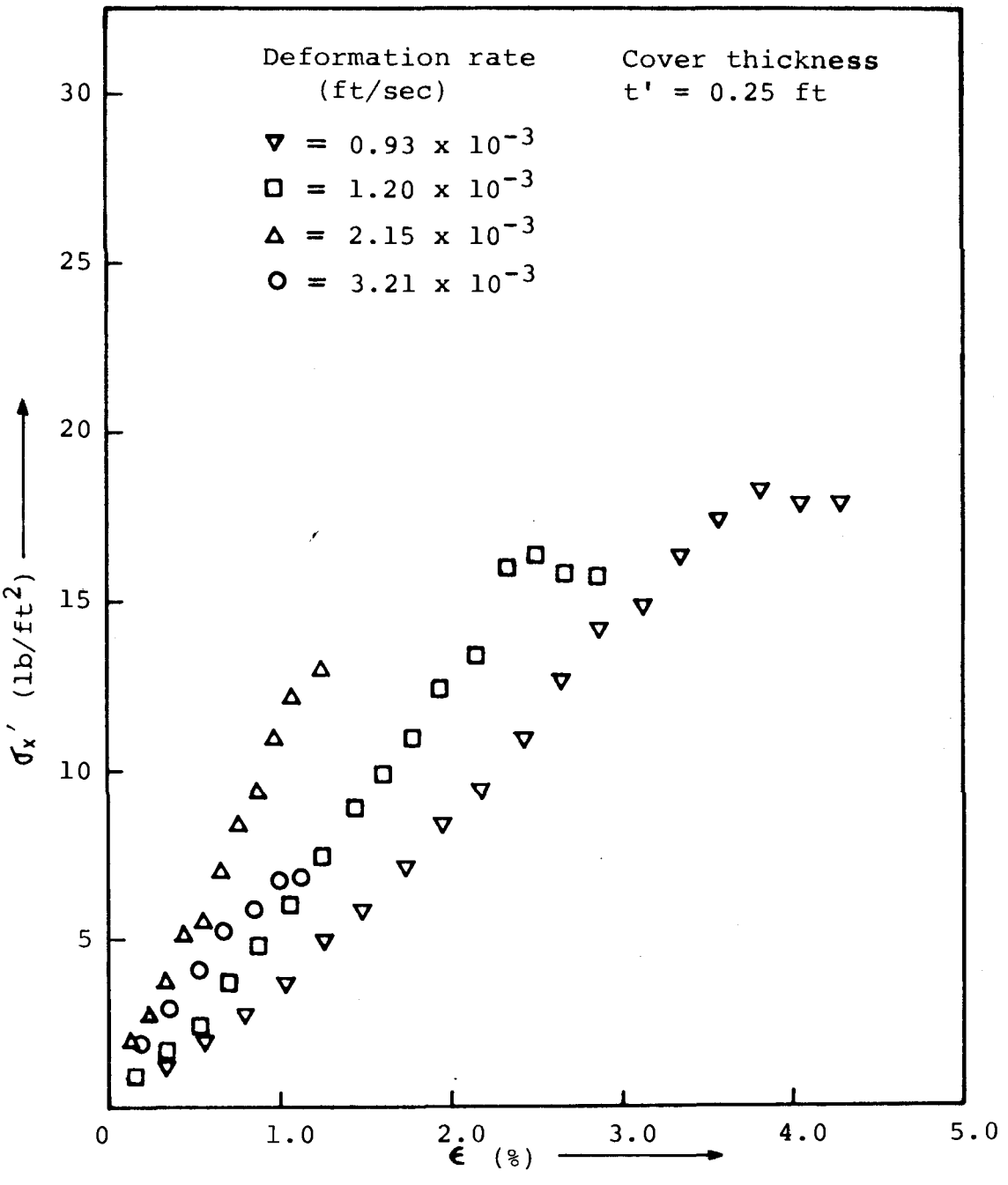

Figure 10. Typical compressive stress-strain curve of fragmented ice cover (t' = 0.25 ft).

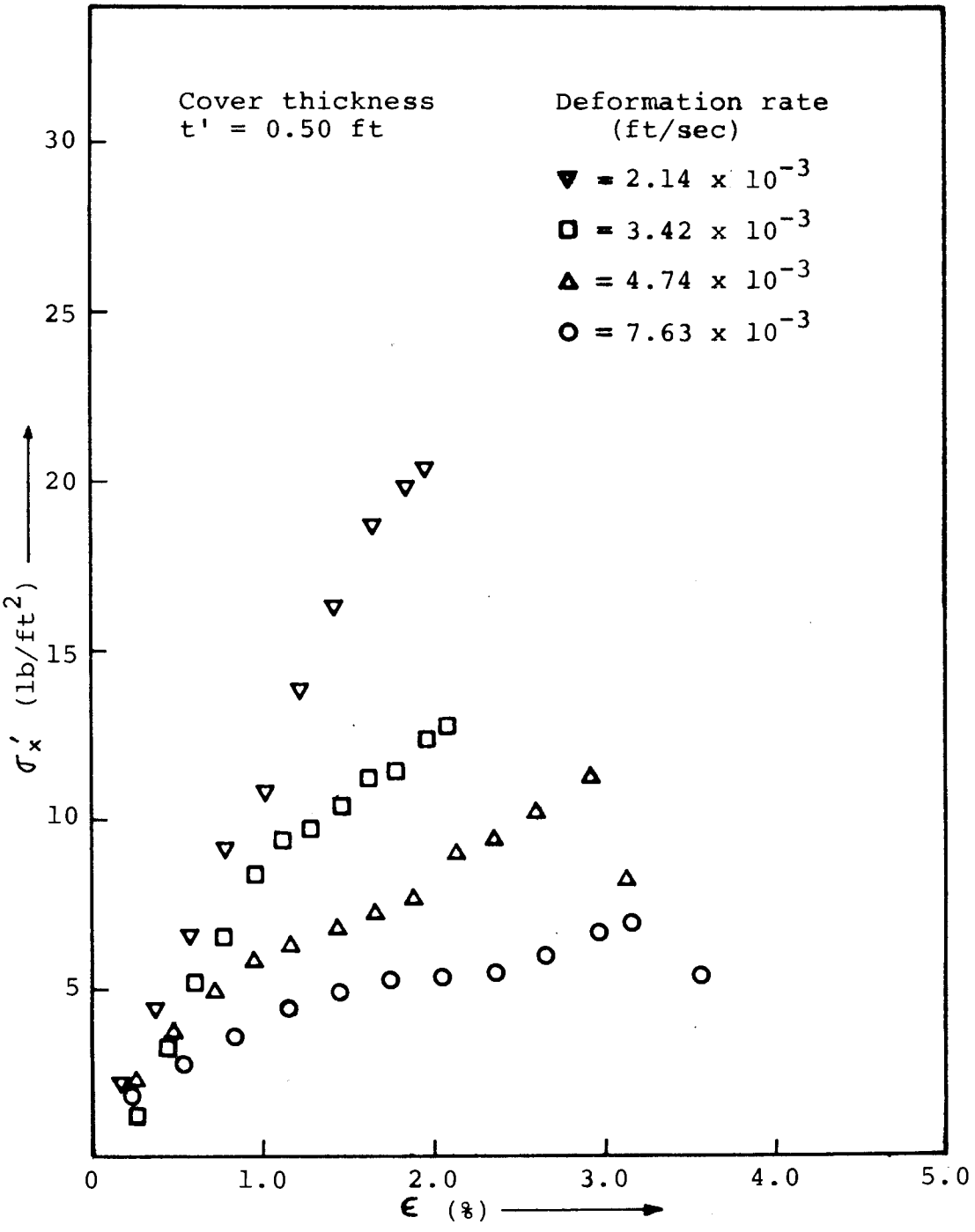

Figure 11. Typical compressive stress-strain curve of fragmented ice cover (t' = 0.50 ft).

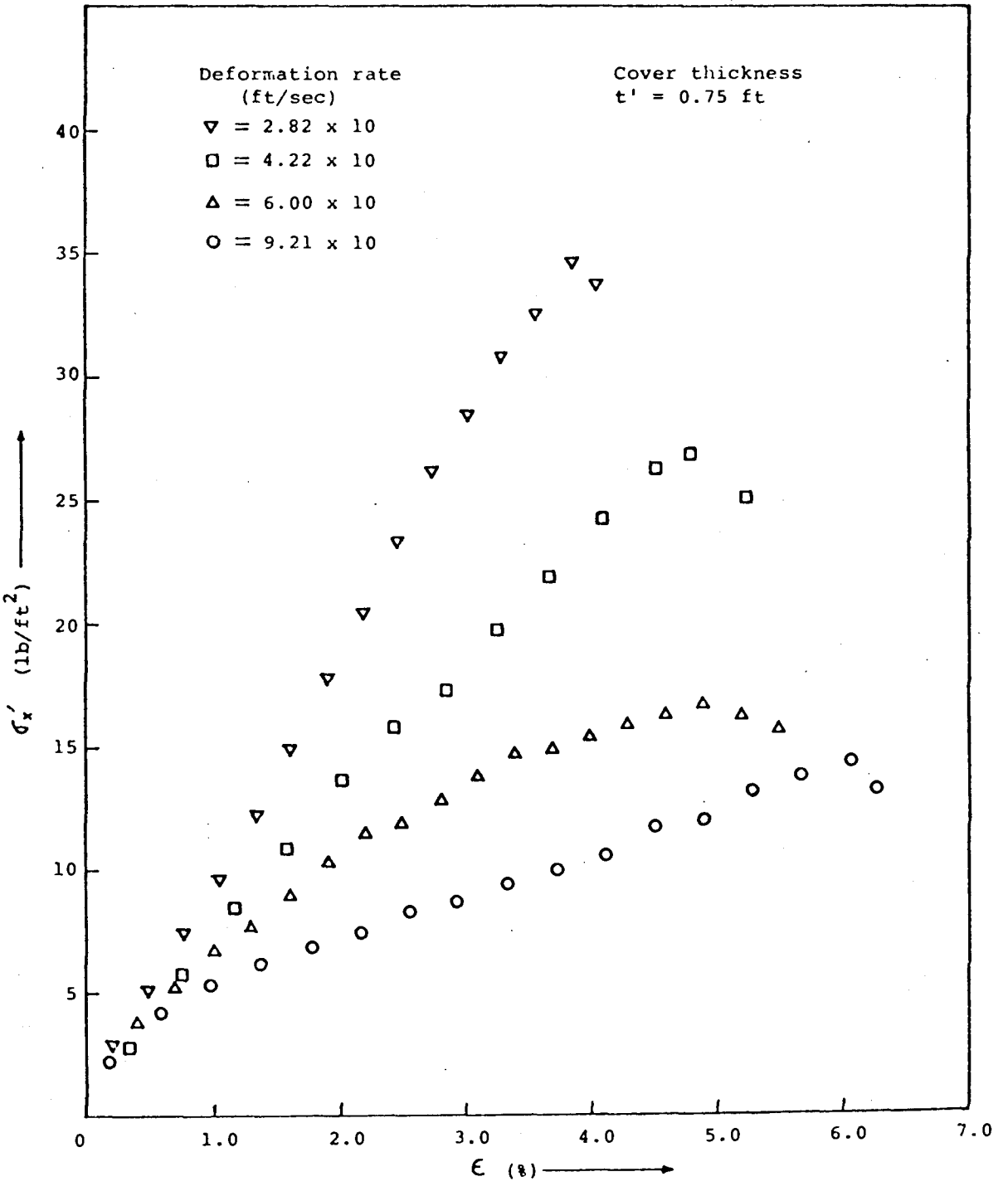

Figure 12. Typical compressive stress-strain curve of fragmented ice cover (t' = 0.75 ft).

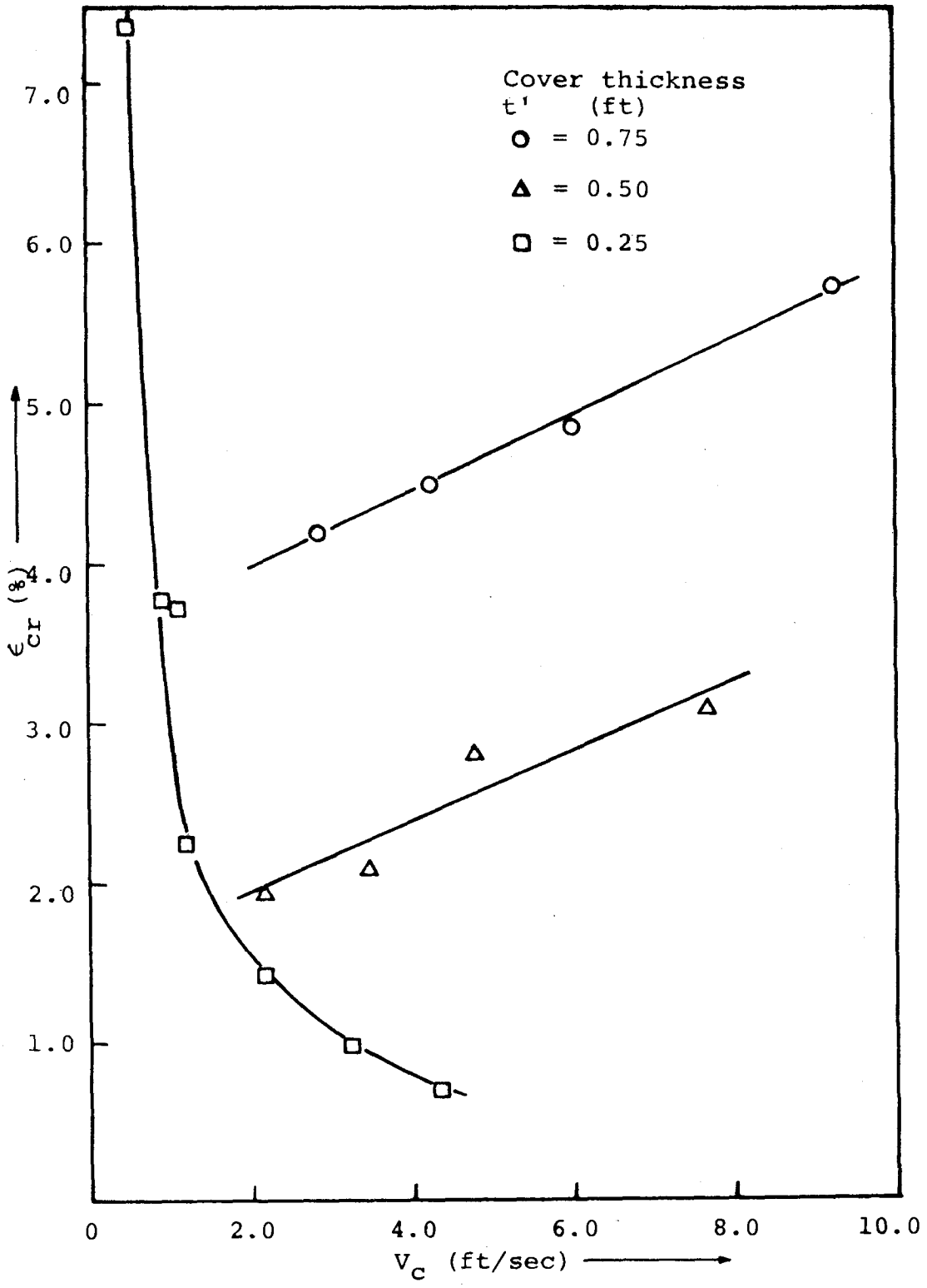

Figure 13. ϵ_{cr} versus V_c for compression tests without preloading.

effect of cover thickness was not investigated here.

(b) Compressive strength-plate velocity relationship. The results of the compression tests without preloading are plotted for the three submerged ice cover thicknesses t' of 0.25, 0.50 and 0.75 ft, as compressive strength obtained at first failure, σ_{cr}, versus plate velocity, V_c, in Figure 14. Similarly to results of previous investigations, σ_{cr} is found initially to decrease with increasing V_c (with a slope of -1 on the log-log plot), but for $V_c > 0.01$ ft/sec, approximately, σ_{cr} appears to become approximately constant. Also, σ_{cr} increases with cover thickness t. However, when σ_{cr}/t is plotted versus V_c as in Fig. 15, the data appear to collapse more or less on a single curve, especially for the two lower values of t investigated, while the data points for t = 0.815 ft (t' = 0.75 ft) remain somewhat higher. When $\sigma_{cr} \times V_c > 0.01$ ft/sec, σ_{cr}/t become more or less constant with an average value of 10 lb/ft^3, approximately.

(c) Comparison of present results with Nakato's results. When the experimental results obtained in the present study are compared with those reported by Nakato in 1976 for similar cover thicknesses (Figure 21 of report by Tatinclaux et al (1976)), the present values of σ_{cr} are found to be significantly lower; at times as much as 50% difference can be observed. No fully satisfactory explanation of such a large discrepancy can be offered. It was verified through consultation with Dr. Nakato that the two series of experiments were performed in practically identical fashion. The only actual difference was that the displacement, and thus speed, of the carriage was actually measured in each of the present experiments while Nakato relied on the calibration of the speed control setting performed at the beginning of the series of experiments. It was verified that such correspondence between dial setting of the carriage remote control and carriage speed did not vary appreciably over a long period of time. Since it was also observed that the carriage speed, for a given dial setting, could be affected by the load applied onto the driving plate, specific experiments were conducted to determine the magnitude of such effect. It was found that the load began to affect the carriage velocity, only when IF exceeded 300 to 350 lbs, beyond the range of Nakato's experiments. The porosity of the covers studied here was found to be in the same narrow range of values as reported by Nakato. The ice blocks used to form the covers were identical in shape and size.

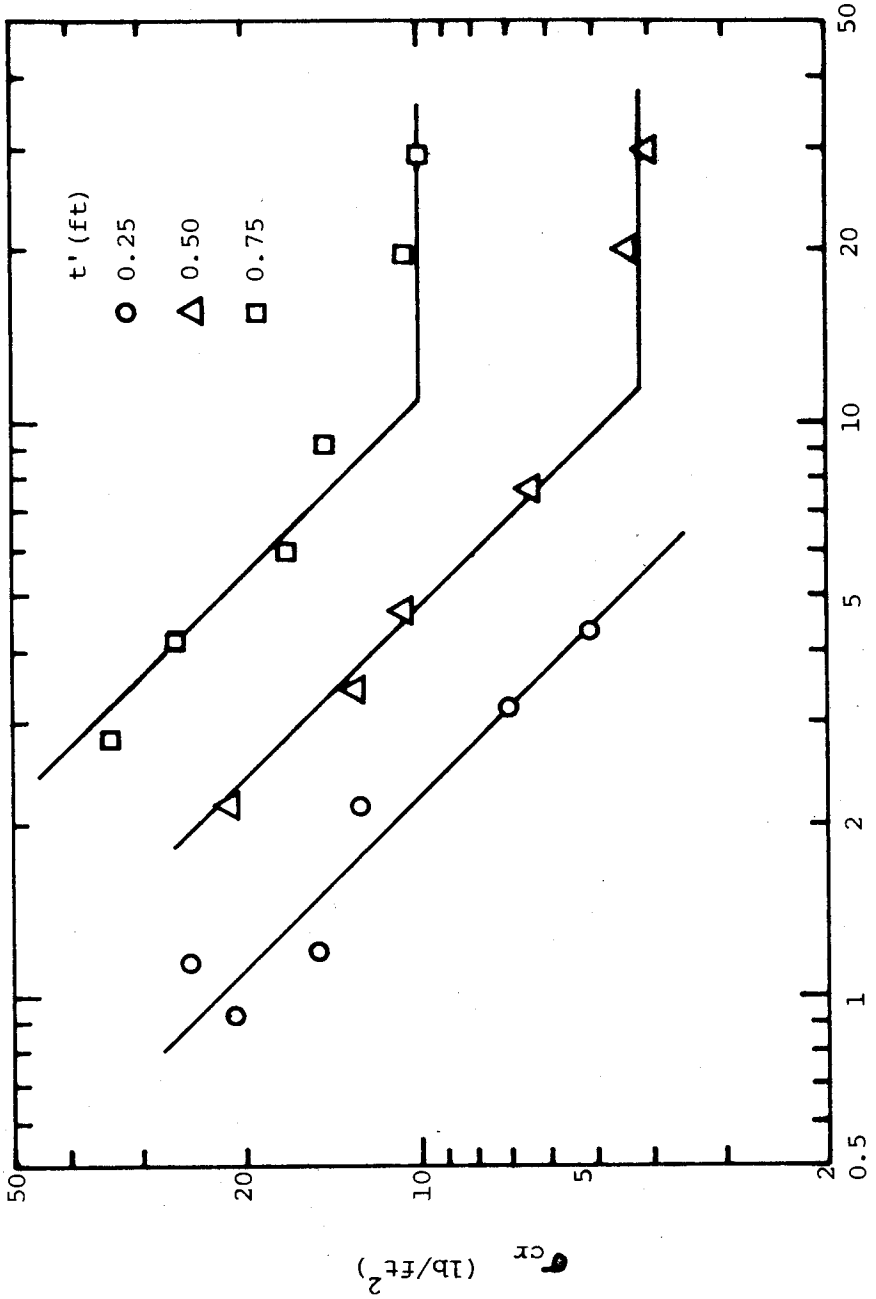

Figure 14. Compressive strength as a function of acting speed in tests without preloading

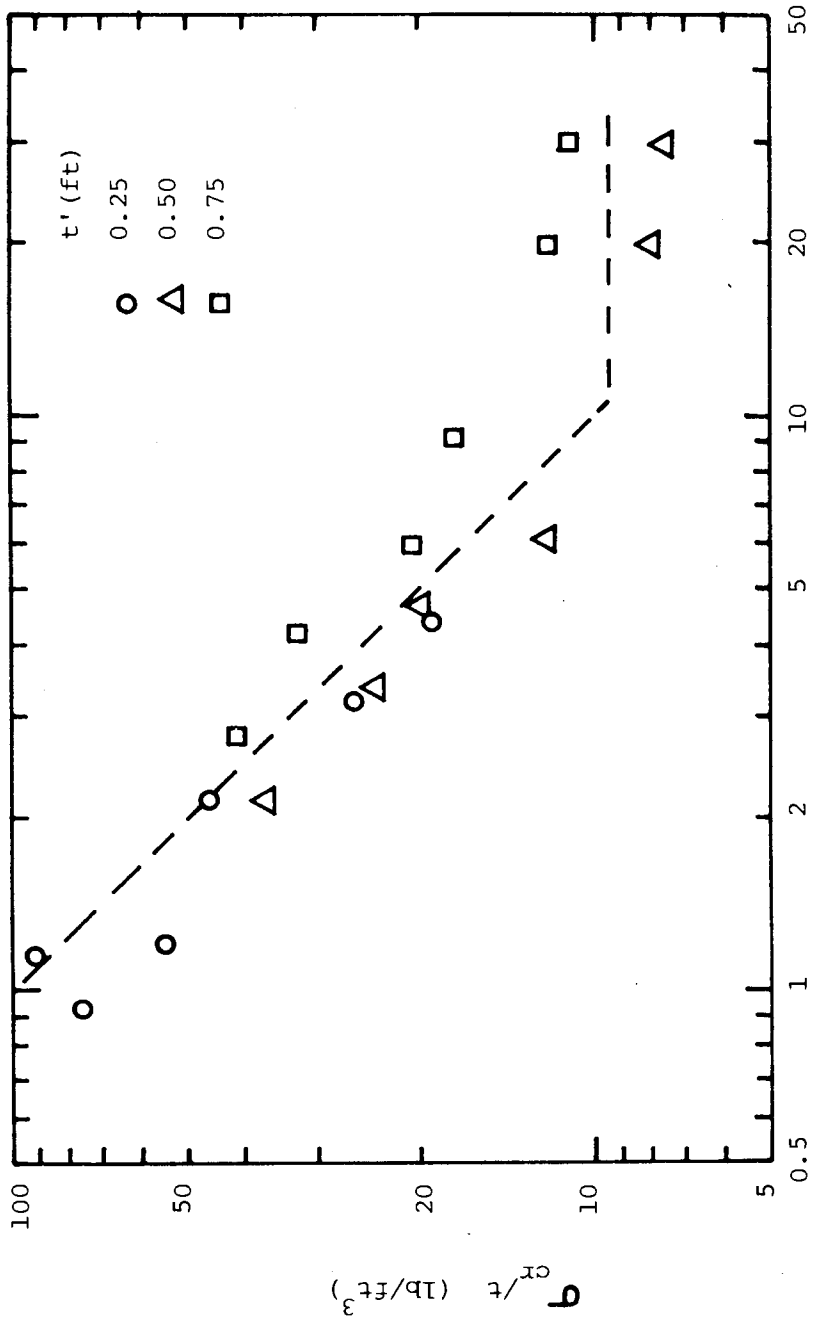

Figure 15. σ_{cr}/t as a function of acting speed in tests without preloading

As a last resort, the differences observed in the results of the two investigations have to be attributed to slight differences in the air temperature in the ice facility. The present thermostat can control the room temperature only within 2° to 3°F at best. That is for a time average temperature of 32°F, the temperature in the room will actually vary between 30° and 33°F, approximately. Even larger variations could occur when one of the blowers in the experimental cold room would become ice covered. Since the pheneomenon studied involves formation of bonds between the individual ice particles it is quite possible that a difference of 1°F in the average air temperature between the two investigations would sufficiently affect the temperature distribution in the upper layer of the floating covers, the formation of interparticle bonds, and as a result, the total strength of the cover. In this respect it should be reemphasized that the values of σ_{cr} presented were averages obtained over eight to ten experiments under identical nominal conditions and that the difference in σ_{cr} between any two such experiments could be as much as 100%.

2. Experiments with preloading. The results of the compression tests with preload applied once (prestrain) and preload applied approximately constant are plotted as σ_{cr} versus V_c in Figure 16 for different preloads varying from 25% to 75% of the failure force as determined from the previous experiments without preload. The values of σ_{cr} are seen to be virtually unaffected by either the magnitude of the preload, or the type of preload; the difference between the results with and without preload are of the same order as the experimental accuracy, even in the case of a cover thickness of 0.75 ft where all the experimental values of σ_{cr} obtained under preloading conditions are slightly larger than those obtained without preloading. The number of experimental data at that thickness remains insufficient to draw definite conclusion. Because of the difficulty in performing the experiments with preload, and the long time required to obtain one data point (which is the average of eight to ten experiments under nominally identical conditions), the efforts were mainly directed towards the effect of preload on σ_{cr} for one cover thickness, namely 0.5 ft, and a relatively few experiments were conducted at a thickness

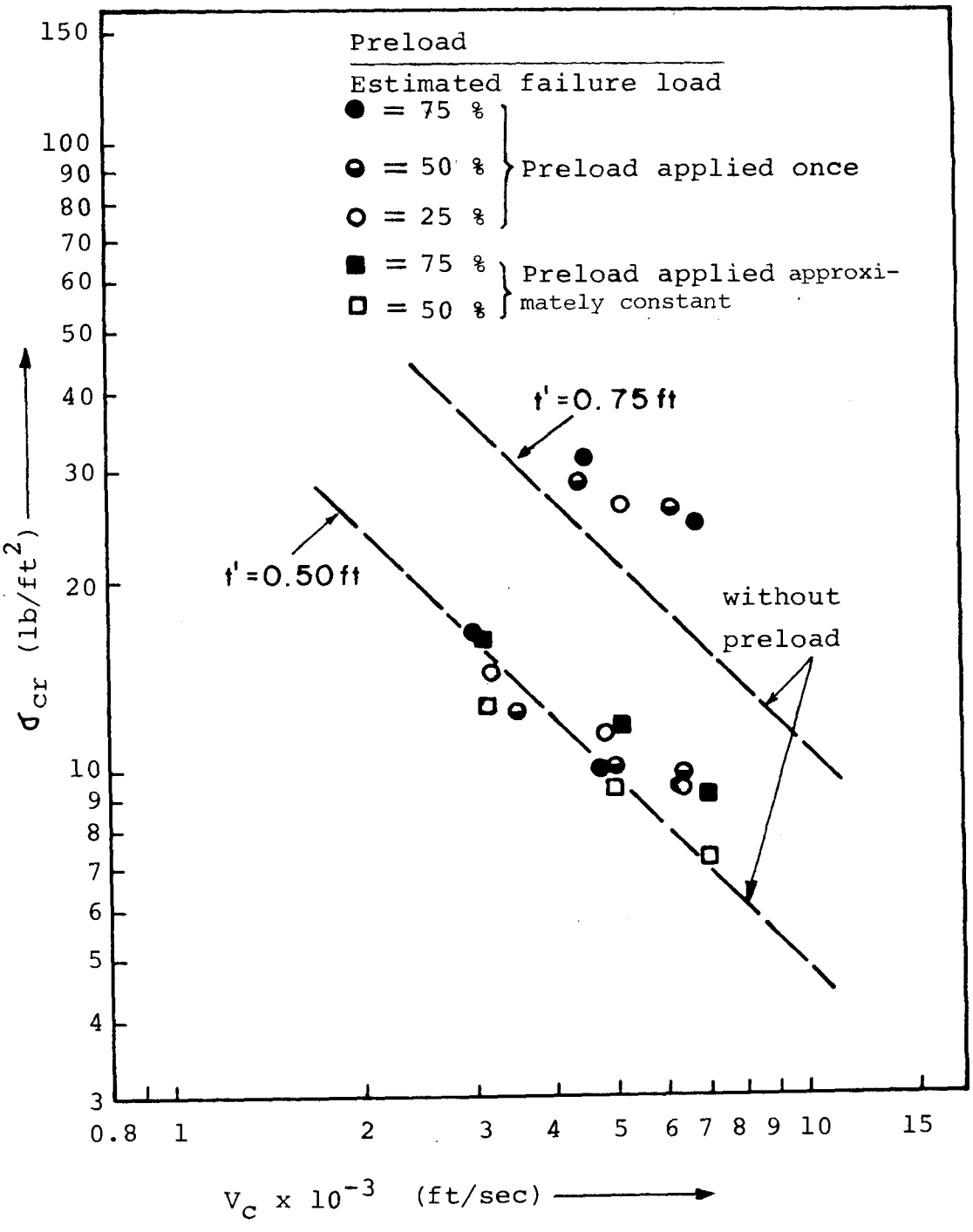

Figure 16. Compressive strength as a function of acting speed in tests with preloading.

of 0.75 ft, only to verify that the conclusions drawn from the results obtained at a thickness of 0.5 ft could be extended to higher cover thicknesses.

III. SHEAR STRENGTH OF FRAGMENTED ICE COVERS

A. Introductory Remarks. From the results of Merino's (1974) shear strength tests, it was found that the shear strength was dependent on the deformation rate, ice cover thickness, ice cover length, size and shape of ice specimen. The dependence on the cover length was believed to be due to the presence of compressive stresses during Merino's experiments. These compressive stresses were attributed to the geometry of the test apparatus and to the manner in which it applied loads to the specimens. In an attempt to eliminate or at least to reduce greatly the effects of the length of the ice cover on shear strength, two other apparatus were used. One was a modified version of the rectangular shear apparatus used by Merino (1974) and the other was a cylindrical shear apparatus. The tests performed in the rectangular shear apparatus and cylindrical shear apparatus are labeled here as direct shear tests and vane shear tests, respectively. Detailed description of the two apparatus is presented later.

In this investigation of the shear strength of floating fragmented ice cover, experiments were conducted under the conditions listed in Table 4.

B. Experimental Units.

1. Rectangular shear apparatus. The shear apparatus, illustrated in Figures 17a,b and 18,consisted of three parts:

(a) Force driving mechanism. A moving vertical I-shape unit with one flange at each extremity, two intermediate smaller vanes,and one center web separated the ice cover into two parts within two rectangular half-compartments fixed to the walls of the tank. Two following walls at the end of the I-shape unit prevented the ice floes from escaping from the test compartments after some displacement of the moving I-shape unit had taken place. The I-shape unit was attached to the motor driven carriage through the moment insensitive dynamometer. The carriage and the

Table 4. Conditions of shear strength tests in rectangular and cylindrical shear apparatus

Test apparatus / Test conditions	Modified rectangular shear apparatus		Cylindrical shear apparatus
Ice sample	** parallelepiped ice blocks	crushed ice	crushed ice
Cover length L (ft)	0.8, 1.2 and 2.0	1.2 and 2.0	1.0
Cover thickness t' (ft)	0.3, 0.5, 0.7 and 0.9	0.25, 0.50 and 0.75	0.25, 0.50 and 0.75
Range of speed V_c (ft/sec)	0.82×10^{-3} to 20.0×10^{-3}	0.65×10^{-3} to 5.47×10^{-3}	0.65×10^{-3} to 5.36×10^{-3}

** These experiments were conducted by T.D. Hsu, research assistant at the Institute of Hydraulic Research.

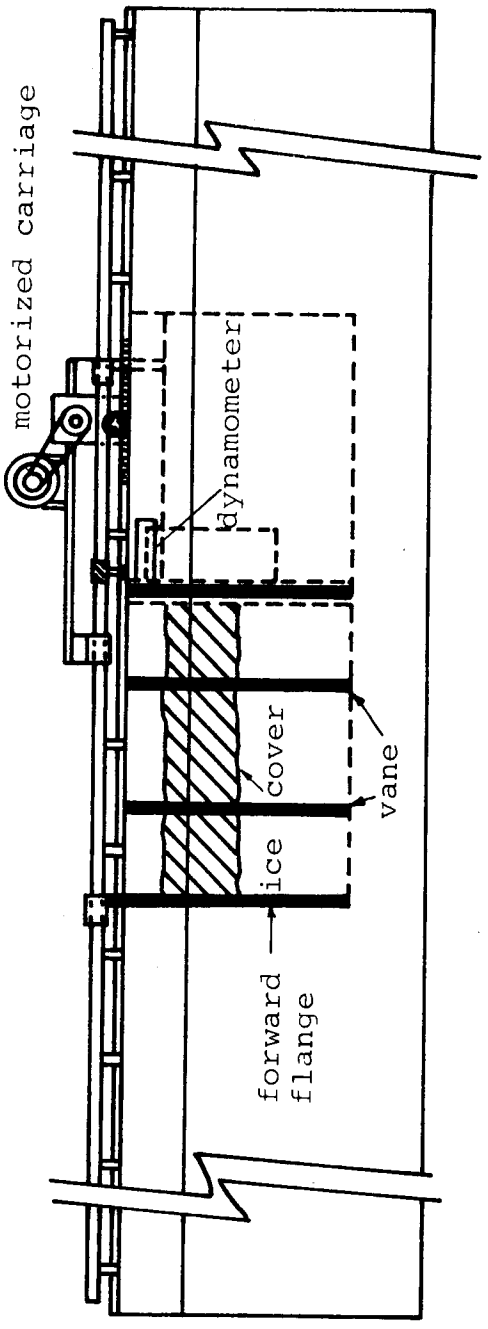

a) Vertical cross section

Figure 17. Schematic rendering of rectangular shear apparatus used in shearing strength tests.

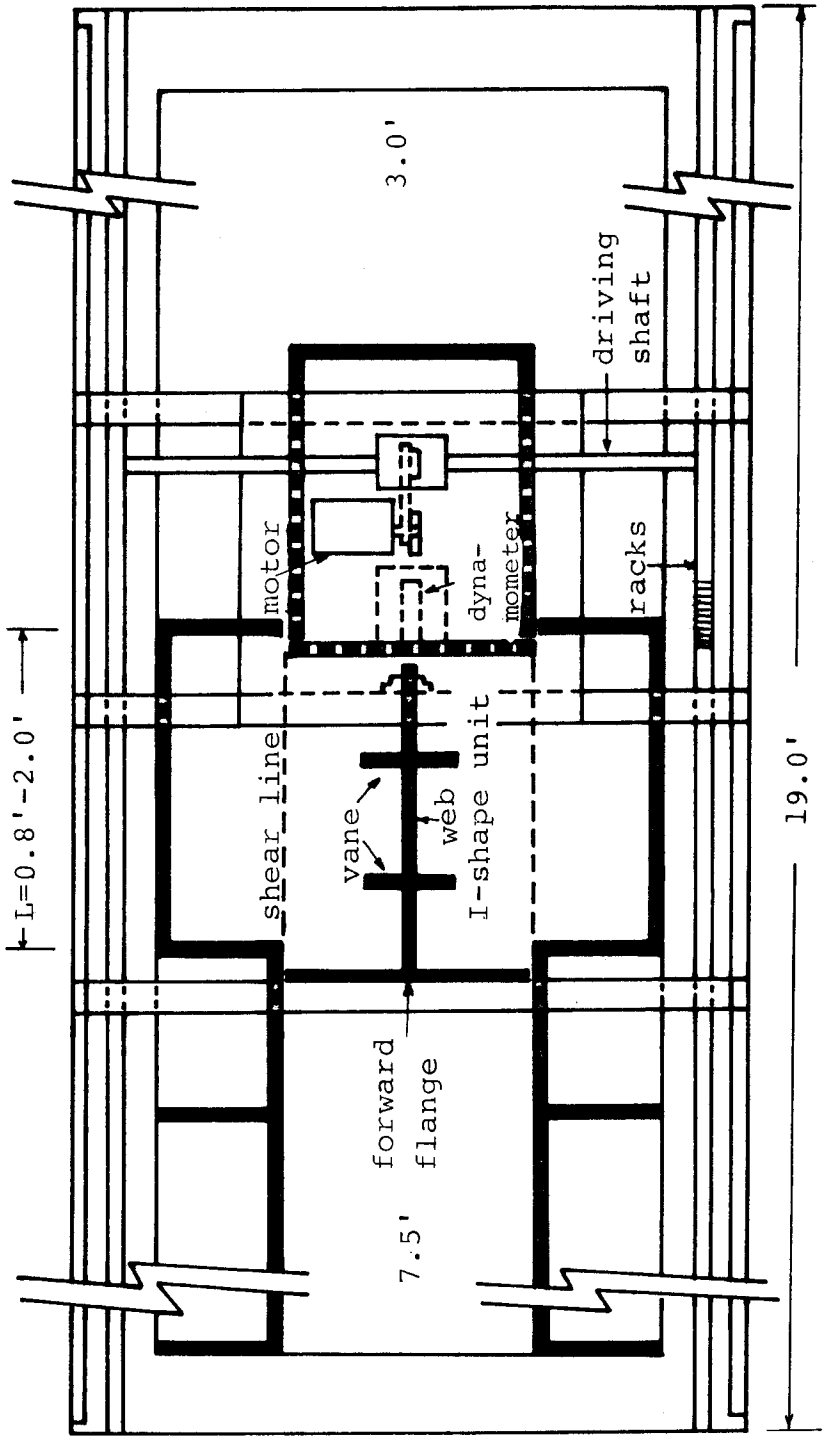

b) Plan view

Figure 17. (Continued).

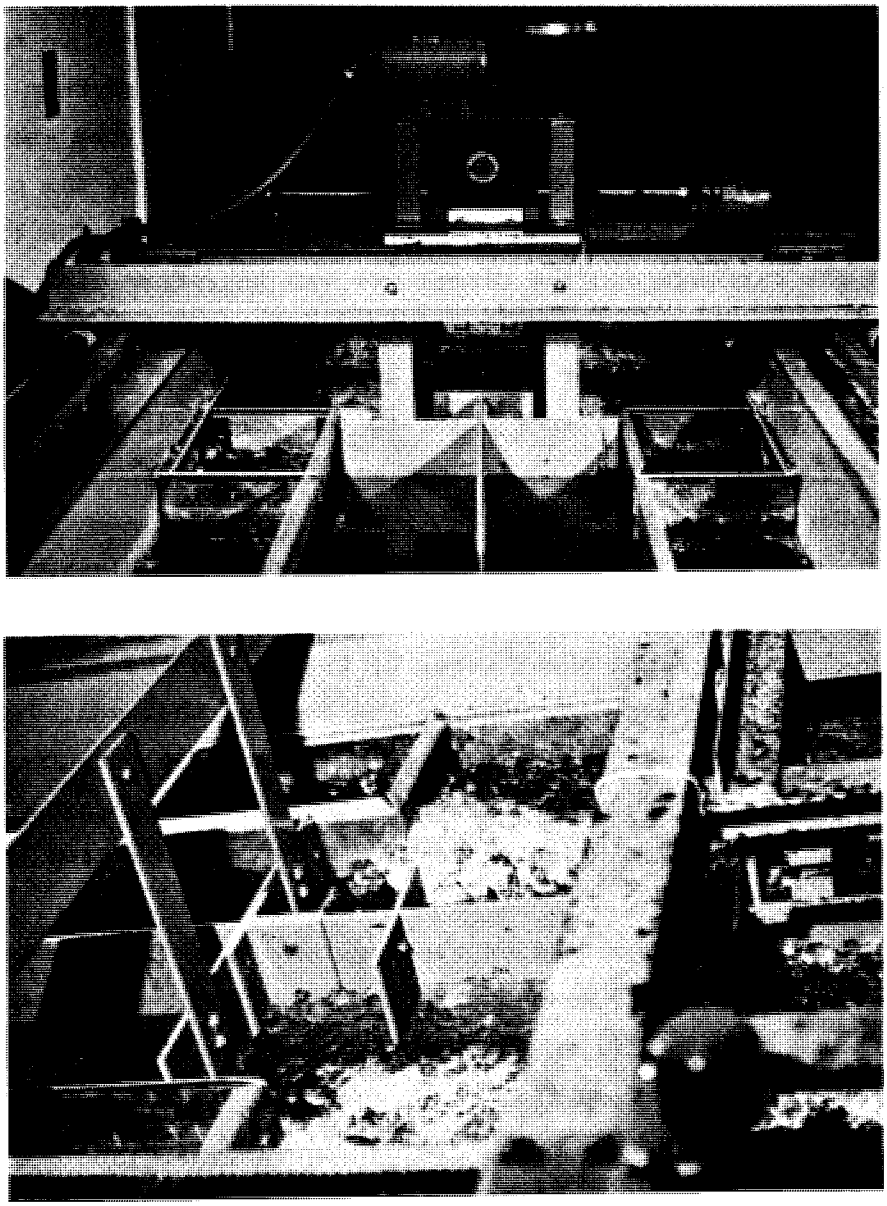

Figure 18. Photographs of rectangular shear apparatus

dynamomter were the same as those used in the compression tests described in section II.

In reassembling Merino's apparatus it was found that the forward flange plate was attached to a cross-beam riding freely on the rails but that the center web was originally bolted onto a cross-beam rigidly attached to the carriage. The question arose whether part of the shear load generated when the carriage was set in motion was transmitted to the carriage itself rather than to the flange plates and the dynamometer. The rigid link between the carriage and the center web was therefore disconnected since sufficient support of the moving part of the apparatus was provided by the arm of the dynamometer attached to one flange plate and by the link connecting the forward flange plate to the free-riding cross beam. It was thus ensured that the shear load was entirely transmitted to the dynamometer.

(b) Force measuring system. One Statham universal transducer cell, Model UC3 and one load cell, Model UL4 were installed in the dynamometer and used to measure the shear force of the fragmented ice cover. One of two load cells, of capacity 200 lbs and 500 lbs, was used depending on the expected magnitude of the shear force. The voltage output of the transducer was amplified by and recorded on the Beckman Dynograph R Type previously used in the compression tests. Calibration ratios are listed in Table 5.

(c) Displacement measuring system. The displacement of the moving I-shape unit was measured by the potentiometer previously described and shown in Figure 5. This set-up was the same as that for the compression tests reported in section II.

2. Cylindrical shear apparatus. A sketch and photographs of this apparatus are shown in Figures 19 and 20, respectively. The cylindrical shear apparatus consisted of:

(a) Rotating mechanism. A cross-shaped vane with radius, R_c = 1.92 in., was attached to an inner rotating axle driven by the 1-hp DC, SCR controlled motor on the carriage of the ice tank through a cone-pulley and a geared speed reducer system. An concentric outer cylinder wall of radius R_o = 5 in. was supported by the rotating axle, but not constrained by it. This outer cylinder was fitted with eight vertical

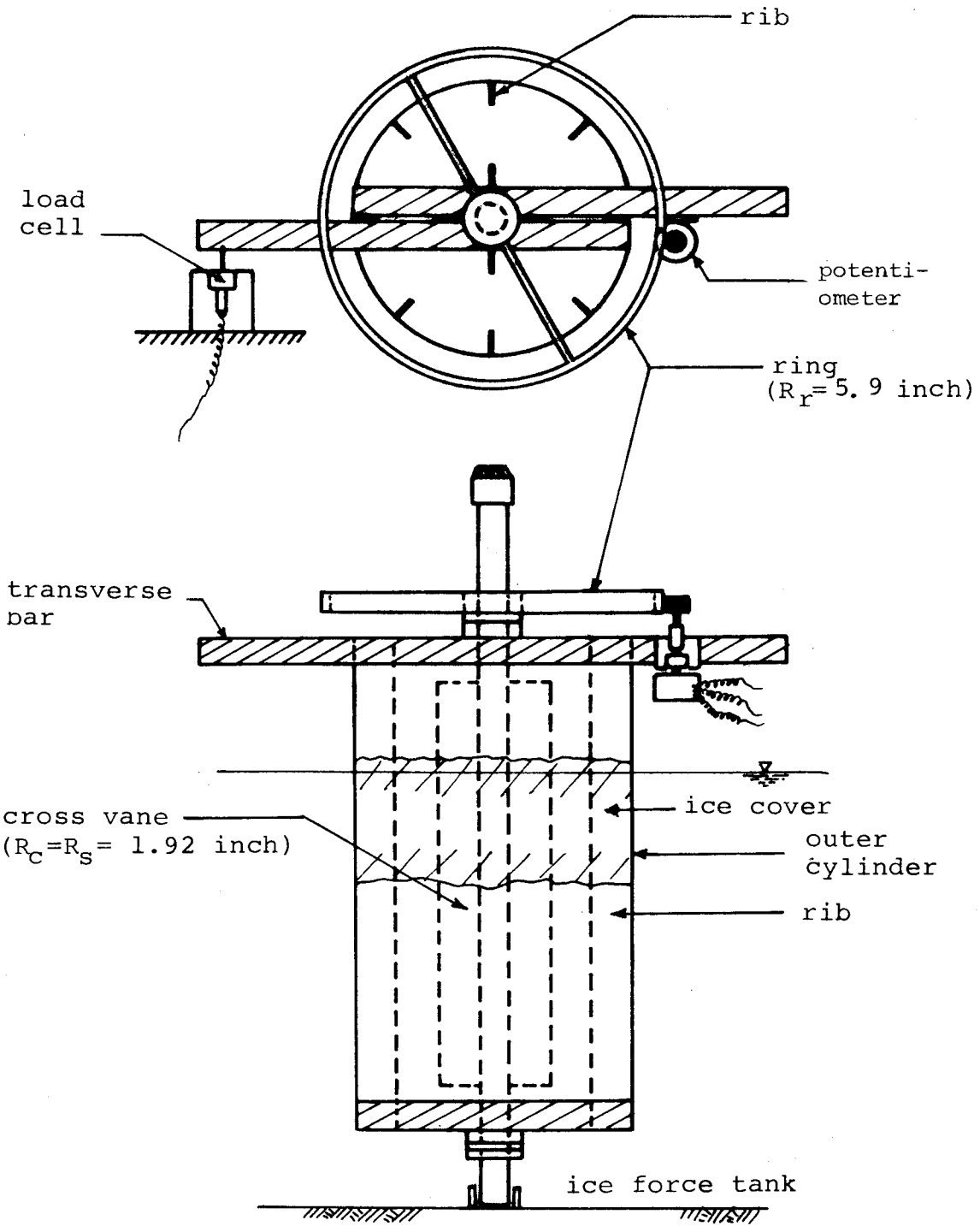

Figure 19 Schematic rendering of cylinderical shear apparatus used in shearing strength tests.

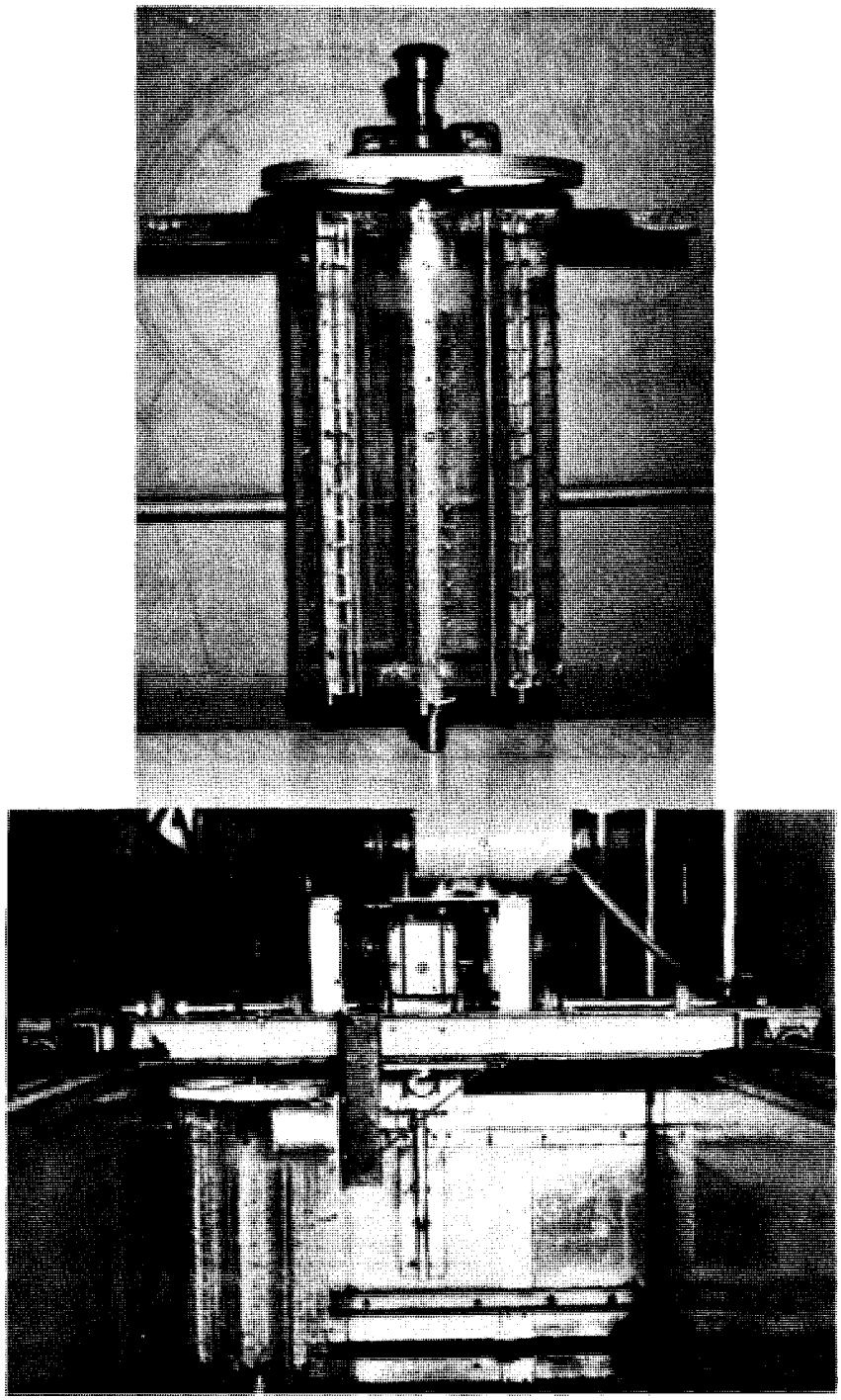

Figure 20. Photographs of cylindrical shear apparatus

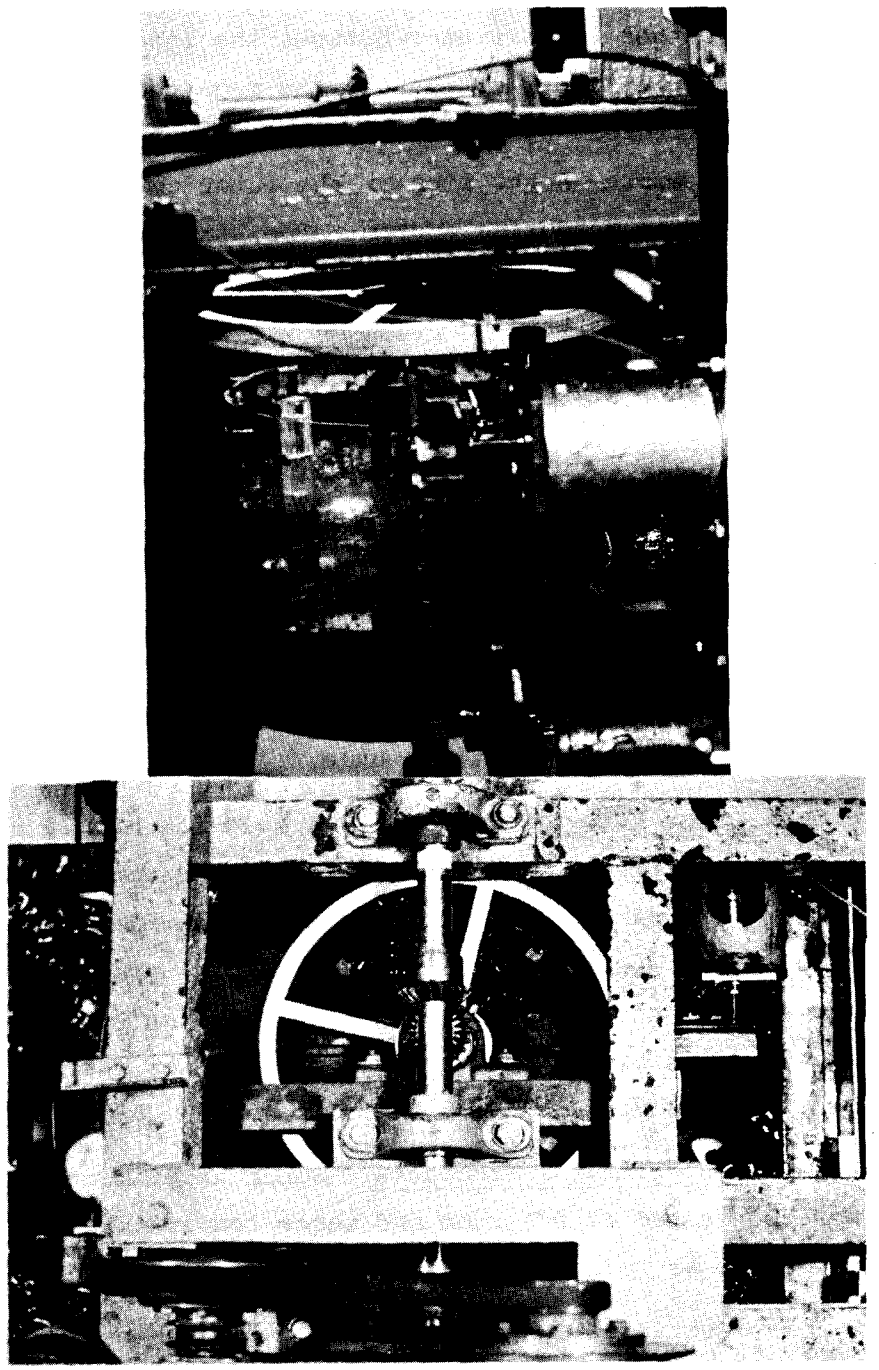

Figure 20. continued

ribs to avoid ice slippage at the boundary of the apparatus. A transverse arm mounted on top of the outer cylinder was connected to a load cell contained in a small round drum attached to the wall of the tank. In order to determine whether the distance between the inner cross vanes and the ribs of the outer cylinder influenced the magnitude of the measured shear strength, two different spacings were used, namely 1.5 in. and 2.5 in., by changing the width of the ribs on the outer cylinder.

(b) Force measuring system. The Statham universal transducer cell, Model UC3, and a 100 lbs load cell, Model UL4, were used to measure the shear force transmitted through the transverse arm when the axle-cross vane system was set to rotate in the ice cover. The voltage output of the transducer was amplified by and recorded on the Beckman Dynograph recorder. The calibration ratios of the load cell are listed in Table 5.

(c) Angular displacement measuring system. A ring of radius R_r = 5.94 inch was attached to the inner rotating axle. The 10-turn potentiometer used in the previous experiments was fixed on the transverse arm with its rotating rubber wheel pressing on the ring. Thus, the displacement $\Delta L = R_r\theta$, and therefore the angular displacement θ was measured as the ring rotated with the inner axle.

C. Test Materials. Parallelepiped ice blocks $1\frac{1}{2}$ inch x $1\frac{1}{4}$ inch x $\frac{5}{16}$ inch manufactured in the IIHR ice-maker and commercial crushed ice were used as test samples in the rectangular shear apparatus. For the cylindrical shear apparatus, only the commercial crushed ice was used as test sample since the ice parallelepipeds were far too big for this apparatus. The particle distribution curve of the crushed ice was obtained by sieving and is shown in Figure 21.

D. Experimental Procedure. Shear experiments of fragmented ice cover were conducted at 0°C room and water temperature. The experimental procedures were as follows:

1. Rectangular shear apparatus. At the beginning of each run, the I-shape unit was moved to its initial position so that the compartment was rectangular. The required quantity of ice floes for the desired cover thickness and cover length were placed in both side compartments. The ice cover was gently agitated to insure uniform thickness. The ice-cover

Table 5 Calibration ratios of force to output voltage for load cells with different capacities. (unit = lb/mv)

Sensitivity / Load cell	0.5 (mv/cm)	1.0 (mv/cm)	2.0 (mv/cm)	5.0 (mv/cm)	10.00 (mv/cm)
500 #	---	17.200	17.125	16.885	16.129
200 #	---	6.900	6.800	6.866	6.866
100 #	2.994	3.048	3.117	3.037	---

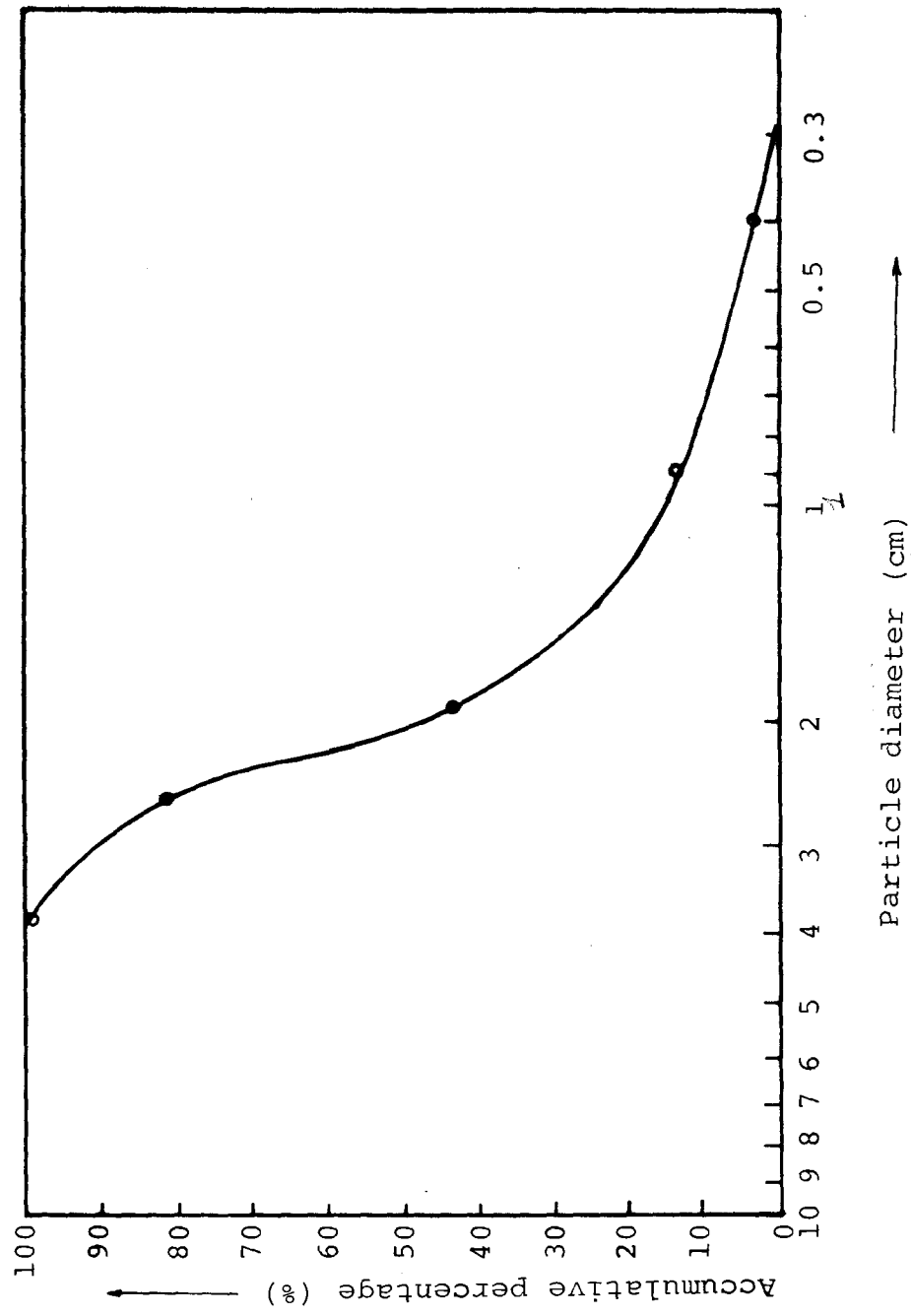

Figure 21. Particle distribution curve of crushed ice.

thickness was measured at four points or more on each side of the I-shape unit by the L-shape staff gage used in the compression tests, to verify that the cover thickness was uniform and of the desired value. Then, the carriage was set in motion at a prescribed speed and stopped when the ice cover failed. The voltage outputs of the force transducer and potentiometer were recorded versus time on a Beckman Dynograph chart.

2. Cylindrical shear apparatus. The required quantity of crushed ice for the desired cover thickness was introduced between the outer cylinder and the inner axle. The transverse arm was set in contact with the load cell. Then, the ice cover was agitated by a rod and measured by a smaller L-shape staff gage. The inner rotating axle with cross-shape vane was set in motion at the desired speed until the ice cover failed. The voltage output of the force transducer and potentiometer were recorded on the Beckman Dynograph as in the previous experiments.

It was observed that the value of the failure force obtained with the cylindrical apparatus were more consistent than those obtained in the rectangular apparatus. Therefore an average of only four runs under identical nominal conditions were performed with the cylindrical apparatus as opposed to eight with the rectangular apparatus.

E. Description and Discussion of Results. The failure shear force of the fragmented ice cover and displacement of the loading apparatus were determined from the force-displacement-time records. Typical records of this type for both rectangular shear apparatus and cylindrical shear apparatus are shown in Figures 22, 23, and 24. Figures 22 and 23 present results in the rectangular shear apparatus with parallelepiped ice blocks and crushed ice, respectively, at various loading speeds. Figure 24 presents results obtained with crushed ice in the cylindrical shear apparatus. The displacement, measured by the potentiometer, is given by the upper trace and the shear force, measured by the load cell, by the lower trace. The time scale is also indicated on the upper edge of the record.

On the records, the trace of the displacement versus time is a straight line indicating that the I-shape unit of the rectangular shear apparatus or the cross vane of the cylindrical shear apparatus moved or rotated at a constant speed. Hence, the fragmented ice cover was sheared under constant deformation rate. The displacement, ΔL, and the corresponding

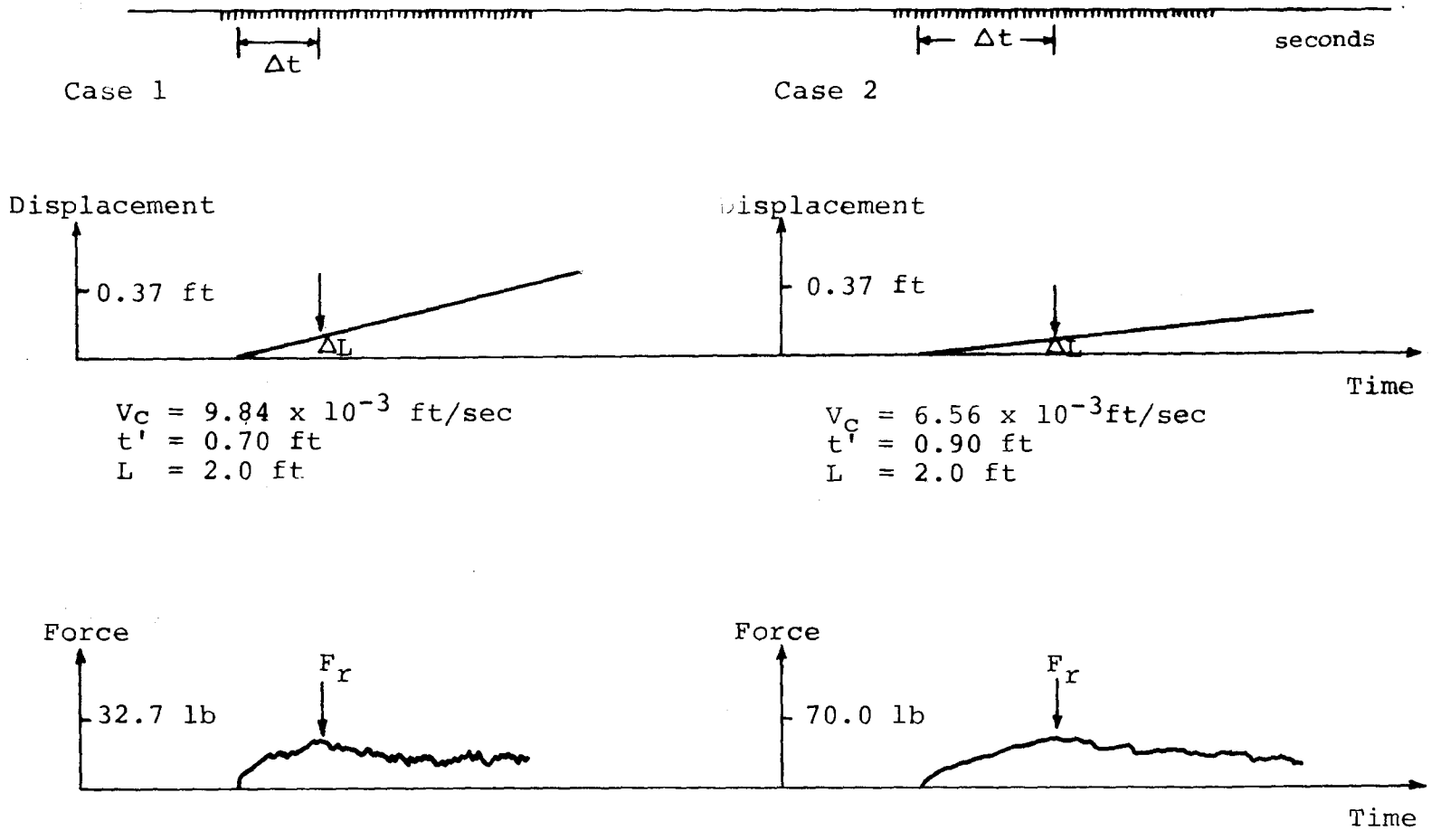

Figure 22. Typical examples of force-displacement-time record for shearing tests in rectangular shear apparatus with parallelepiped ice blocks.

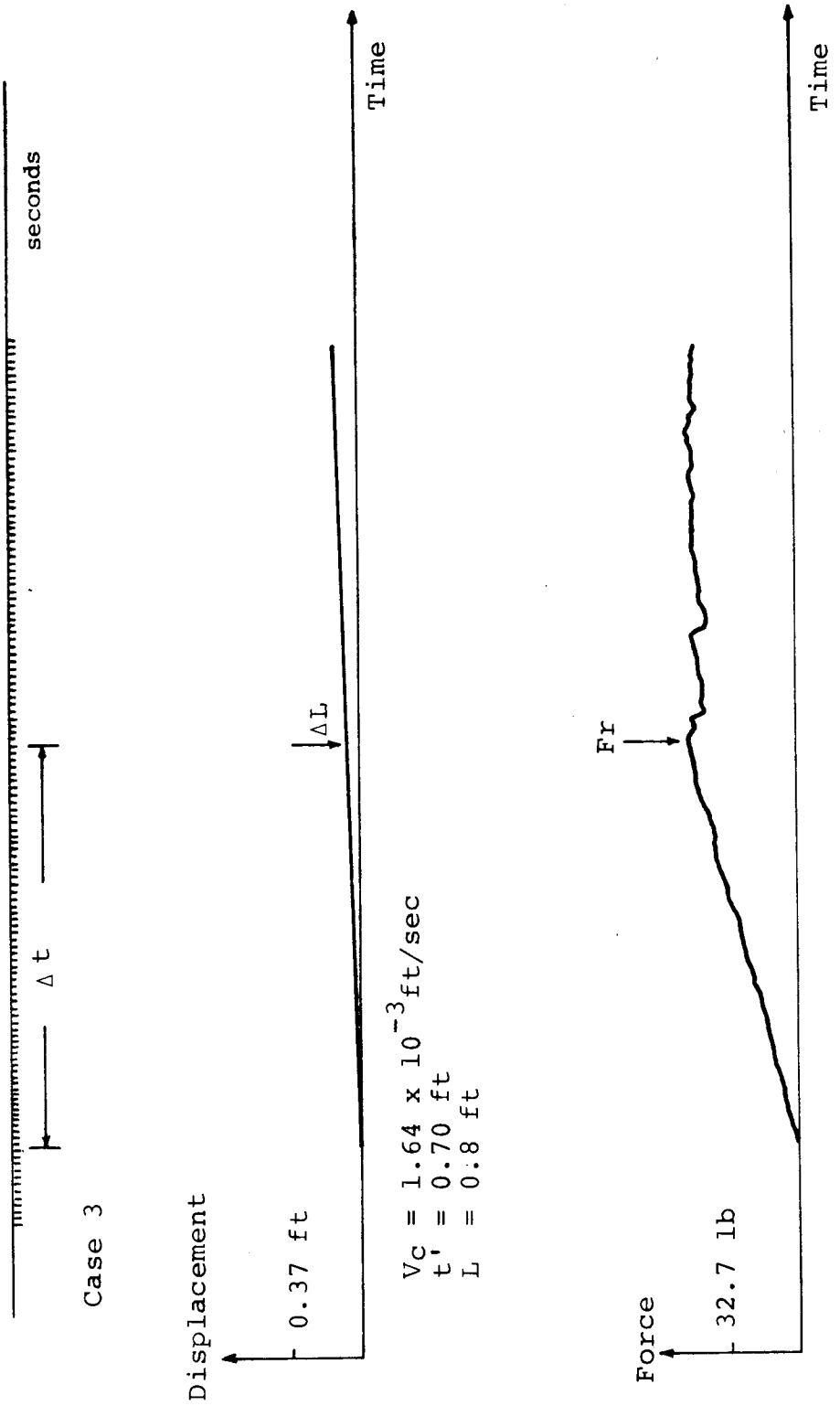

Figure 22. (continued)

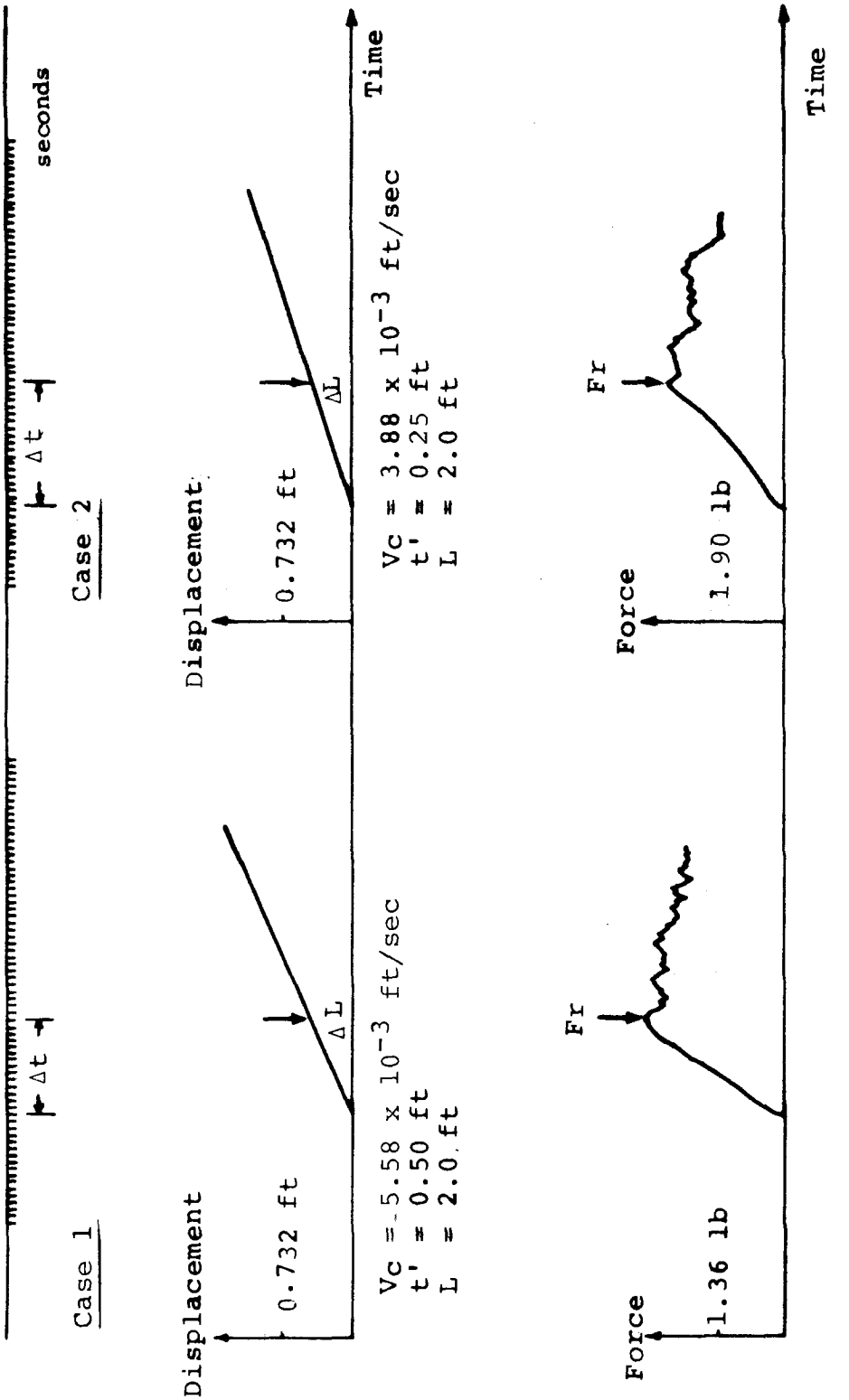

Figure 23. Typical examples of force-displacement-time record for shearing tests in rectangular shear apparatus with crushed ice.

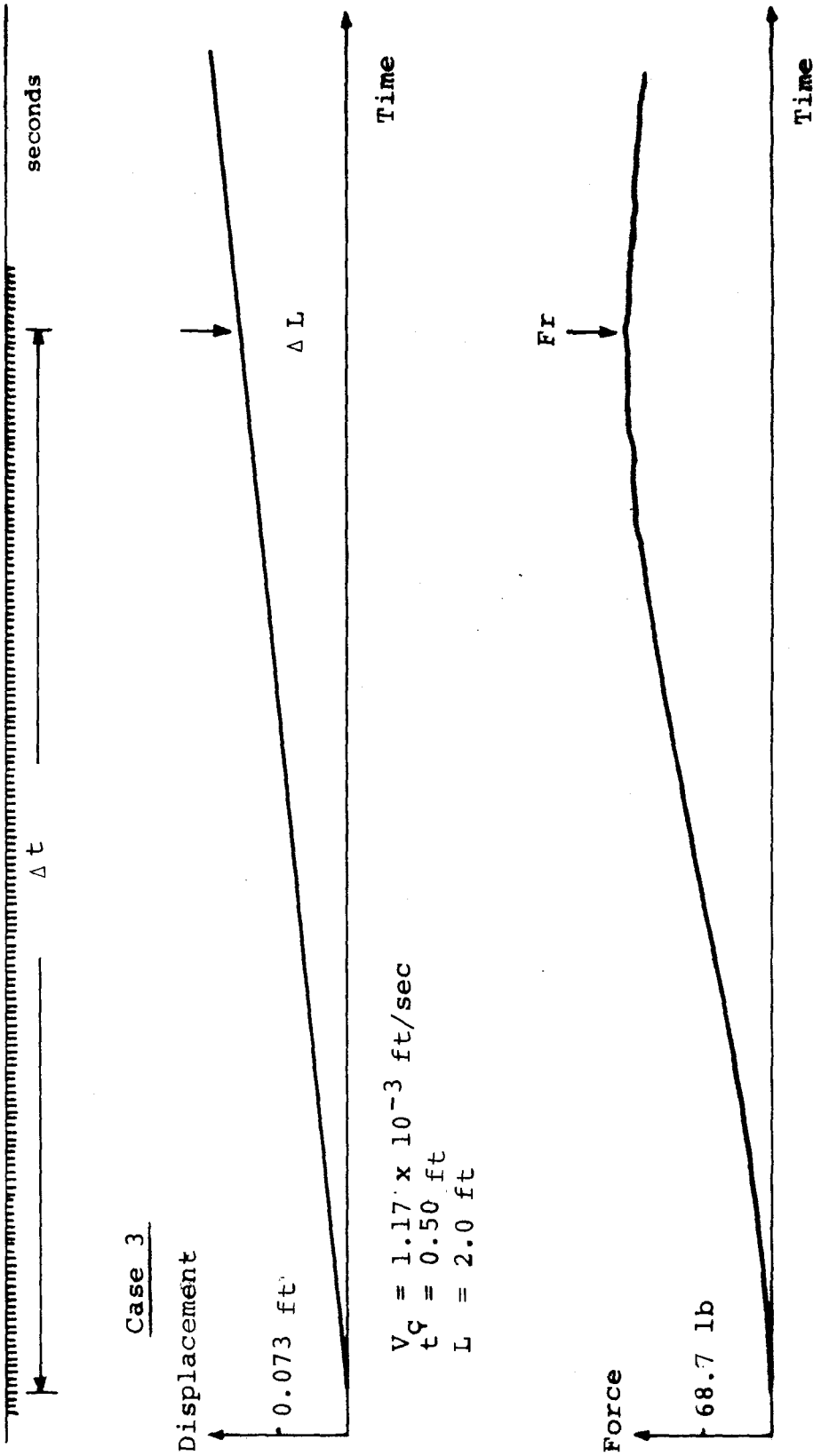

Figure 23. (continued)

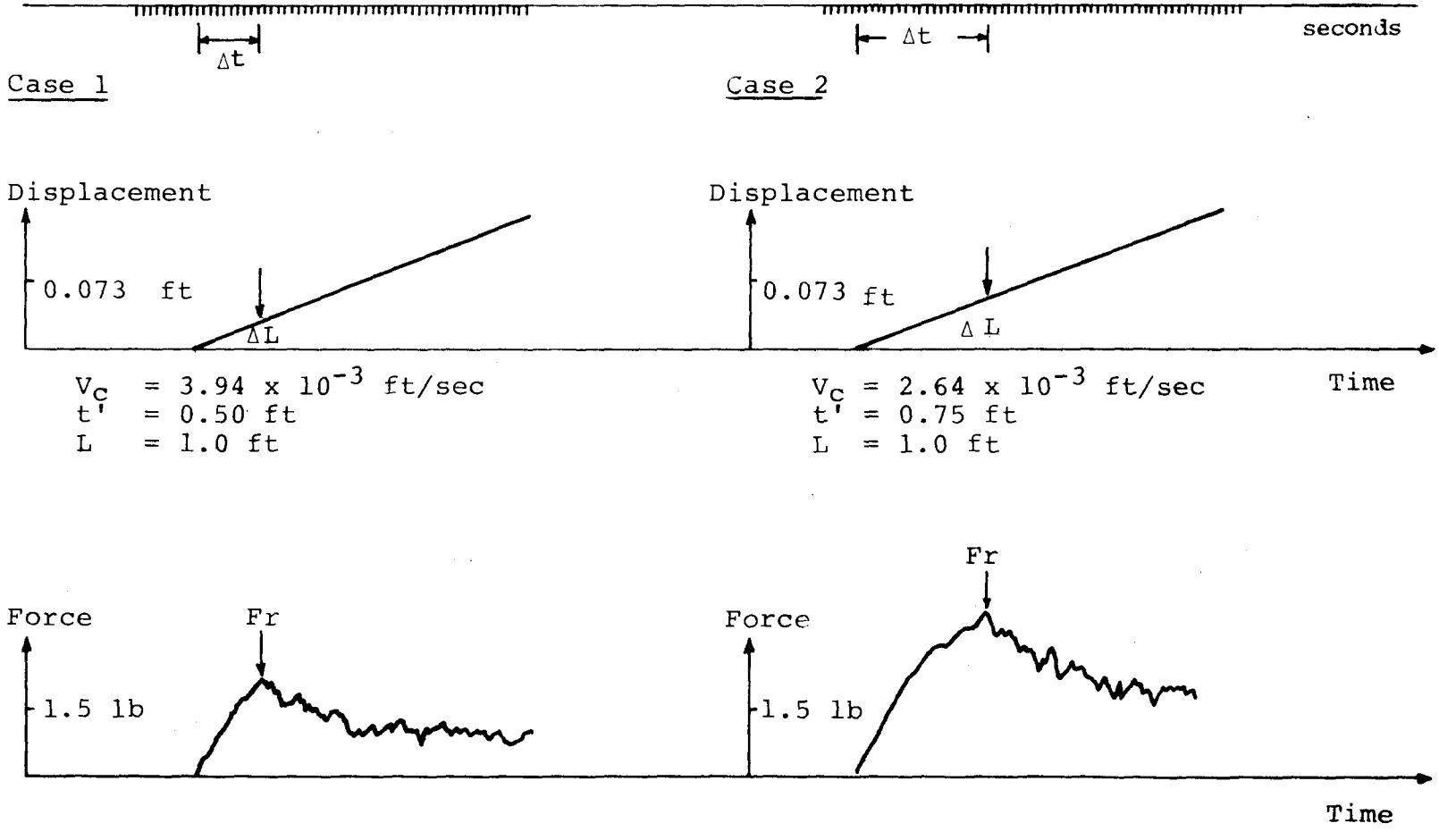

Figure 24. Typical examples of force-displacement-time record for shearing tests in cylindrical shear apparatus with crushed ice.

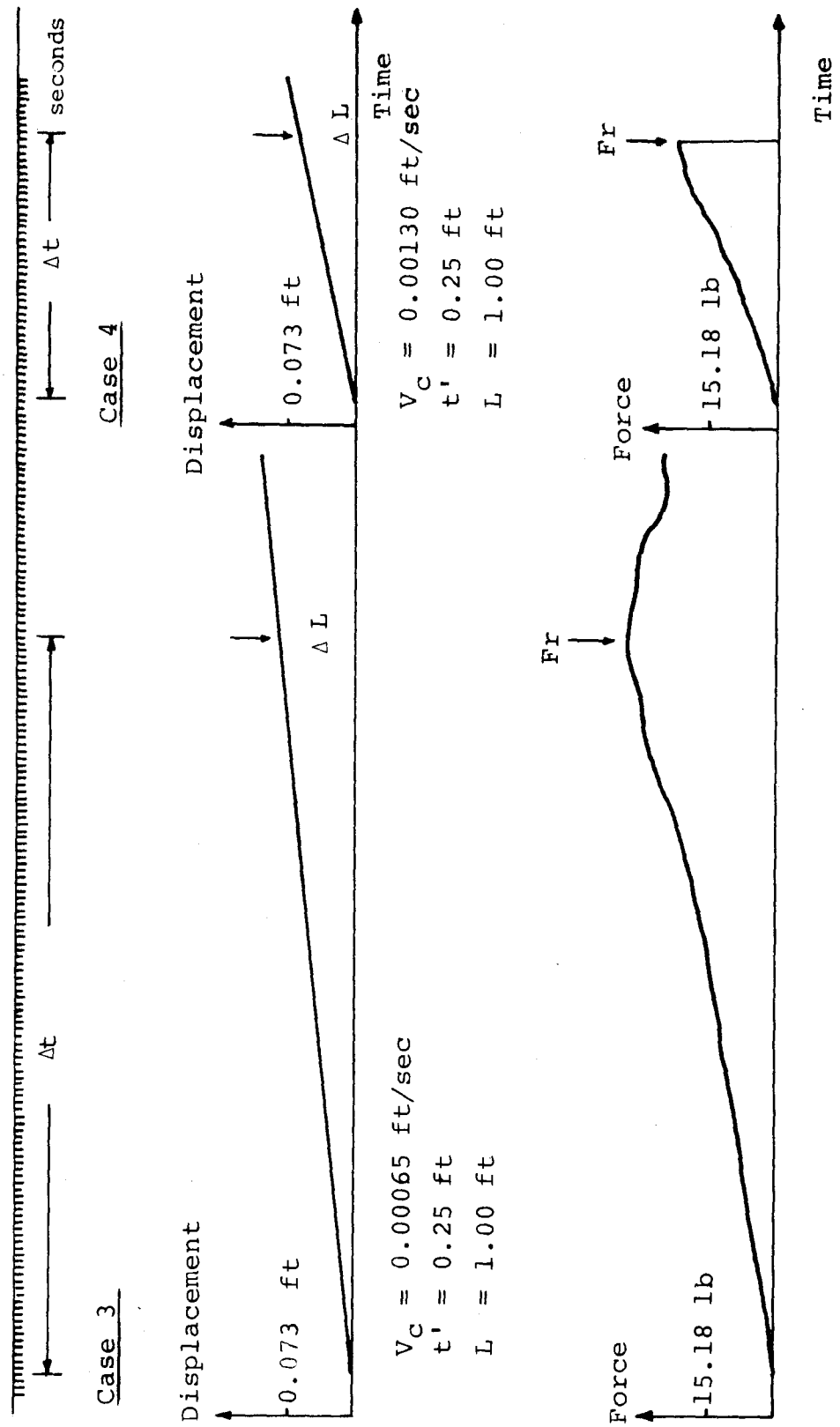

Figure 24. (continued)

time lapse, Δt, from the beginning of the experiment to the occurrence of failure were measured.

From Figures 22, 23, and 24, it is seen that the force-versus-time records are similar for the two types of ice (crushed or in blocks) and the two shear apparatus used. In general, the shear force applied to the fragmented ice cover increased almost linearly with displacement until it reached some maximum point, then decreased gradually or irregularly, indicating failure of the cover. The maximum value of force recorded was taken as the failure shear force, F_r. It was found that at high loading speed (cases 1 and 2 in Figures 22 to 24) the shear force after failure of the ice cover varied more irregularly and decreased more rapidly than at low loading speed (case 3 in Figures 22 to 24). This difference is believed to be due to the larger relative motion between the ice particles along the failure surface at high loading speed. Besides, it was observed that during the low speed experiments formation of weld-cohesive bonds between ice particles occurred and thus limited the relative motion and orientation between the ice particles. Hence, the force versus time trace appears to be smoother at lower loading speeds.

It was also observed that an abrupt drop in the shear force as case 4 in Figure 24 happened occasionally during shear tests in the cylindrical shear apparatus. However, this was only accidental, since, as is characteristic of soil shear tests, there should be a residual shear along the failure surface of the fragmented ice cover. Hence, the shear force should decrease after failure to a certain constant residual value, and not decrease abruptly to zero. The occasional abrupt drop is believed to result from an unbalance in the force distribution attributed to the ribs on the outer cylinder. A torsion force existed at this boundary and was released when the ice cover failed. The release of the torsion force caused the outer cylinder boundary to rotate in the direction opposite to that of the cross-vane and, hence, caused the transverse arm to lose contact with the load cell, resulting in a zero output.

By comparing the force-displacement-time records obtained in the shearing tests, Figures 22 through 24, and in the compression test, Figure 8, it is found that some difference exists between these two kinds of records. In the compression tests, after failure of the ice cover,

several force peaks more or less than the failure strength occurred when the compression test continued, because of rearrangement of the ice floes and thickening of the ice cover led. However, in the shearing tests, the shear force decreased after the failure of the ice cover and no more force peaks appeared, since only the residual shear force remained, which was approximately constant in each experiment with the circular apparatus, but decreased in the rectangular apparatus with decreasing shearing area which accompanied increasing displacement along the failure surface of the ice cover.

F. Data Calculation and Presentation

1. Calculation of shear strength. The shear strength of the fragmented ice cover is defined as the ratio of failure shear force to the area on which the shear force acts. Since the ways for applying shear force are different between the rectangular shear apparatus and the cylindrical apparatus, the failure shear strength is thus calculated with different equations, as follows:

(a) In the tests with rectangular shear apparatus, the average failure shear strength along the failure surface is calculated from the equation

$$\tau = \frac{\sum_{i=1}^{n} \frac{F_{ri}}{2(L - \Delta L_i) \times t}}{n} \tag{4}$$

where

F_{ri} = maximum force recorded at i-th run

L = ice cover length

ΔL_i = displacement of the I-shape unit, or the ice cover when the first peak force appeared at i-th run

t = ice cover thickness

n = number of runs performed under nominally identical conditions

Since the ice cover was sheared on two faces in these tests, the area on which the shear force acted, was calculated as $2(L - \Delta L_i)t$ as in (4). This area calculation is different from that of Merino's (1974), in which the area was calculated as $2Lt$. It was found in the present experiments that ΔL can be as large as 18.8% of the initial ice cover length,

L, and should not be neglected in calculating the shearing area. Therefore, the value calculated by Equation 4 will be greater than that in Merino's results.

(b) In the tests with the cylindrical shear apparatus, the recorded force, F_r, is the balance force from the torque caused by the shear force along the failure surface of the ice cover with respect to the center of the inner rotating axle. Therefore, the average failure shear strength along the failure surface was calculated from the equation

$$\tau = \frac{\sum_{i=1}^{n} \frac{F_{ri} \times R}{2\pi R_s^2 t}}{n} \tag{5}$$

where

R = distance from the axis of load cell to the center of the inner rotating axle.

R_s = mean radius of the failure surface

It was observed in the experiments that R_s in (5) was always equal to the radius of the cross vane R_c.

2. Calculation of the acting speed. In the rectangular shear apparatus, the speed of the I-shape unit on the ice cover is defined as $V_c = L/\Delta t$, which is the same as that defined in the compression tests. In the cylindrical shear apparatus, the tangential speed, V_c, of the cross-shape vane is defined as

$$V_c = \frac{\frac{\Delta L}{R_r} \times R_c}{\Delta t} \tag{6}$$

where

R_c = radius of cross vane = R_s

R_r = radius of ring attached to the rotating axle

3. Calculation of the failure strain. The failure strain of ice cover by the rectangular shear apparatus was defined as $\varepsilon_\tau = \frac{\Sigma \Delta L_i}{nL}$, which is the same as that defined in the compression tests. However, the failure strain obtained in tests with the cylindrical shear apparatus was defined as

$$\varepsilon_\tau = \frac{\sum_{i=1}^{n} \Delta L_i}{n\ 2\pi R_r} = \frac{\sum_{i=1}^{n} \theta_i}{2\pi n} \tag{7}$$

where θ_i was the angular displacement of the vanes when failure occurred.

The results of the shearing tests are summarized in Tables 6, 7 and 8, which correspond to tests using parallelepiped ice blocks, crushed ice in the rectangular shear apparatus, and crushed ice in the cylindrical shear apparatus, respectively.

G. Graphical Presentation of Results

1. Relation between shear strength, strain and acting speed. From the force-displacement-time records, the shear strength along the failure surface, τ', experienced by the ice cover at any time, T, and the corresponding strain, ε, could be determined. Typical strength-strain plots are shown in Figures 25 through 28. Figures 25 and 27 show $\tau' - \varepsilon$ curves for various acting speeds, but constant values of ice cover thickness and length. Figures 26 and 28 present $\tau' - \varepsilon$ curves for various ice cover thicknesses, but constant speeds and cover lengths. Figures 25 and 26 present results obtained with the rectangular shear apparatus, while Figures 27 and 28 present results obtained with the cylindrical shear apparatus.

From Figures 25 and 27, it is clear that the shear strength and the strain of ice cover at yield increase with decreasing speed of the I-shape unit or rotating cross-vane. This phenomenon was again explained by Merino (1974) by the effect of bonding. Accordingly, the larger failure shear strengths and accompanying larger failure strains at the smaller acting speed result from cohesive bonds having more time to develop at lower speeds as the ice cover is sheared. At higher rates of deformation, on the other hand, the cohesive bonds cannot develop as completely, and the cover strength is reduced.

From Figures 26 and 28, it is seen that the shear strength at yield is also affected by the ice-cover thickness. The shear strength increases with increasing cover thickness. The strain at yield in Figure 26 (rectangular shear apparatus) also increases with increasing cover thickness. The results obtained with the cylindrical apparatus (Figure 28) show also an increase of ε_τ with both decreasing speed and increasing cover thickness.

2. Relation between failure strain, acting speed and ice cover thickness. Curves of failure strain ε_τ against acting speed V_c for

Table 6 Summary of experimental results from shearing tests in rectangular shear apparatus using parallelepiped ice blocks

No.	t' (ft)	L (ft)	V x 10^{-3} (ft/sec)	τ (lb/ft^2)
RP1	0.3	2.0	0.82	52.75
RP2	0.3	2.0	1.64	20.00
RP3	0.3	2.0	3.28	8.33
RP4	0.3	2.0	6.54	4.17
RP5	0.3	2.0	9.84	4.17
RP6	0.3	2.0	13.12	2.50
RP7	0.3	2.0	16.39	2.10
RP8	0.3	2.0	19.67	2.10
RP9	0.5	2.0	6.82	59.20
RP10	0.5	2.0	1.64	45.90
RP11	0.5	2.0	3.28	15.00
Rp12	0.5	2.0	6.54	3.65
RP13	0.5	2.0	9.84	3.15
RP14	0.5	2.0	13.12	3.00
RP15	0.5	2.0	16.39	3.35
RP16	0.5	2.0	19.67	3.65
RP17	0.7	2.0	0.82	63.90
RP18	0.7	2.0	1.64	34.50
RP19	0.7	2.0	3.28	12.60
RP20	0.7	2.0	6.54	8.30
RP21	0.7	2.0	9.84	8.20
RP22	0.7	2.0	13.12	4.75
RP23	0.7	2.0	16.39	4.60
RP24	0.7	2.0	19.67	4.60

Table 6 Continued

No.	t' (ft)	L (ft)	V x 10^{-3} (ft/sec)	τ (lb/ft^2)
RP25	0.90	2.0	0.82	over
RP26	0.90	2.0	1.64	50.80
RP27	0.90	2.0	3.28	49.70
RP28	0.90	2.0	6.54	11.70
RP29	0.90	2.0	9.84	6.70
RP30	0.90	2.0	13.12	5.00
RP31	0.90	2.0	16.39	4.20
RP32	0.90	2.0	19.67	3.50
RM1	0.30	1.2	0.82	34.70
RM2	0.30	1.2	1.64	16.25
RM3	0.30	1.2	3.28	15.00
RM4	0.30	1.2	6.56	9.03
RM5	0.30	1.2	9.84	6.90
RM6	0.30	1.2	13.12	4.72
RM7	0.30	1.2	16.39	4.60
RM8	0.30	1.2	19.67	4.60
RM9	0.50	1.2	0.82	62.50
RM10	0.50	1.2	1.64	31.30
RM11	0.50	1.2	3.28	14.60
RM12	0.50	1.2	6.56	9.30
RM13	0.50	1.2	9.84	6.90
RM14	0.50	1.2	13.12	6.30
RM15	0.50	1.2	16.39	5.40
RM16	0.50	1.2	19.67	5.40
RM17	0.70	1.2	0.82	94.10
RM18	0.70	1.2	1.64	49.40
RM19	0.70	1.2	3.28	21.30
RM20	0.70	1.2	6.56	7.90

Table 6 Continued

No.	t' (ft)	L (ft)	V x 10^{-3} (ft/sec)	ζ (lb/ft^2)
RM21	0.70	1.2	9.84	9.40
RM22	0.70	1.2	13.12	6.00
RM23	0.70	1.2	16.39	5.40
RM24	0.70	1.2	19.67	4.90
RM25	0.90	1.2	0.82	***
RM26	0.90	1.2	1.64	***
RM27	0.90	1.2	3.28	56.00
RM28	0.90	1.2	6.56	16.20
RM29	0.90	1.2	9.84	12.40
RM30	0.90	1.2	13.12	9.30
RM31	0.90	1.2	16.39	9.30
RM32	0.90	1.2	19.67	9.30
RS1	0.30	0.8	0.82	95.20
RS2	0.30	0.8	1.64	51.70
RS3	0.30	0.8	3.28	18.80
RS4	0.30	0.8	6.56	8.30
RS5	0.30	0.8	9.84	6.70
RS6	0.30	0.8	13.12	4.80
RS7	0.30	0.8	16.39	4.80
RS8	0.30	0.8	19.67	2.30
RS9	0.50	0.8	0.82	91.20
RS10	0.50	0.8	1.64	58.40
RS11	0.50	0.8	3.28	29.10
RS12	0.50	0.8	6.56	12.50
RS13	0.50	0.8	9.84	10.40
RS14	0.50	0.8	13.12	8.40
RS15	0.50	0.8	16.39	6.25
RS16	0.50	0.8	19.67	5.25

*** Force exceeds load cell capacity

Table 6 Continued

No.	t' (ft)	L (ft)	V x 10^{-3} (ft/sec)	τ (lb/ft^2)
RS17	0.70	0.8	0.82	103.60
RS18	0.70	0.8	1.64	65.50
RS19	0.70	0.8	3.28	26.80
RS20	0.70	0.8	6.56	13.40
RS21	0.70	0.8	9.84	8.90
RS22	0.70	0.8	13.12	8.90
RS23	0.70	0.8	16.39	6.70
RS24	0.70	0.8	19.67	6.70
RS25	0.90	0.8	o.82	112.50
RS26	0.90	0.8	1.64	62.50
RS27	0.90	0.8	3.28	33.50
RS28	0.90	0.8	6.56	18.50
RS29	0.90	0.8	9.84	13.90
RS30	0.90	0.8	13.12	11.60
RS31	0.90	0.8	16.39	11.60
RS32	0.90	0.8	19.67	11.60

Note RP: results for L = 2.0 ft.
RM: results for L = 1.2 ft.
RS: results for L = 0.8 ft.

*** Force exceeds load cell capacity

Table 7 Summary of experimental results from shearing tests in rectangular shear apparatus with crushed ice

No.	t' (ft)	L (ft)	V x 10^{-3} (ft/sec)	τ (lb/ft^2)	ϵ_z (%)
RL1	0.25	2.0	0.65	76.06	10.33
RL2	0.25	2.0	1.24	51.37	9.43
RL3	0.25	2.0	2.65	21.21	5.80
RL4	0.25	2.0	3.88	11.38	3.68
RL5	0.25	2.0	5.47	7.11	3.05
RL6	0.50	2.0	0.65	***	***
RL7	0.50	2.0	1.24	129.32	9.00
RL8	0.50	2.0	2.65	56.22	5.53
RL9	0.50	2.0	3.88	36.08	5.31
RL10	0.50	2.0	5.47	27.36	4.82
RL11	0.75	2.0	1.24	***	***
RL12	0.75	2.0	2.65	137.84	10.98
RL13	0.75	2.0	3.88	93.36	10.43
RL14	0.75	2.0	5.47	70.50	8.01
RS1	0.25	1.2	0.65	40.55	7.47
RS2	0.25	1.2	1.24	17.35	6.59
RS3	0.25	1.2	2.65	10.31	4.19
RS4	0.25	1.2	3.88	5.25	3.75
RS5	0.25	1.2	5.47	3.34	3.24
RS6	0.50	1.2	0.65	120.79	12.77
RS7	0.50	1.2	1.24	43.82	8.16
RS8	0.50	1.2	2.65	23.44	6.07
RS9	0.50	1.2	3.88	11.83	6.76
RS10	0.50	1.2	5.47	8.31	5.37

Table 7 Continued

No.	t' (ft)	L (ft)	V x 10^{-3} (ft/sec)	τ (lb/ft^2)	ϵ_z (%)
RS11	0.75	1.2	0.65	207.47	18.89
RS12	0.75	1.2	1.24	100.88	13.31
RS13	0.75	1.2	2.65	42.51	8.96
RS14	0.75	1.2	3.88	26.84	8.09
RS15	0.75	1.2	5.47	22.66	7.24

Note RL: results for L = 2.0 ft.
RS: results for L = 1.2 ft

*** Force exceeds load cell capacity

Table 8 Summary of experimental results from shearing tests in cylindrical shear apparatus with crushed ice cubes

No.	t' (ft)	V x 10^{-3} (ft/sec)	τ (lb/ft^2)	ϵ_τ (%)
CS1	0.25	0.65	60.97	6.07
CS2	0.25	1.30	37.61	4.51
CS3	0.25	2.64	19.89	3.75
CS4	0.25	3.94	12.22	4.27
CS5	0.25	5.36	4.89	3.16
CS6	0.50	0.65	107.97	5.65
CS7	0.50	1.30	65.44	4.28
CS8	0.50	2.64	26.62	3.78
CS9	0.50	3.94	18.77	3.76
CS10	0.50	5.36	10.49	5.06
CS11	0.75	0.64	205.16	6.34
CS12	0.75	1.30	111.12	5.40
CS13	0.75	2.64	39.10	4.13
CS14	0.75	3.94	24.21	3.66
CS15	0.75	5.36	11.32	3.65
CW1	0.25	0.64	42.38	4.45
CW2	0.25	1.30	24.58	5.57
CW3	0.25	2.64	15.36	3.75
CW4	0.25	3.94	11.22	2.31
CW5	0.25	5.36	5.77	4.65
CW6	0.50	0.64	123.70	4.66
CW7	0.50	1.30	75.22	3.49
CW8	0.50	2.64	30.25	3.61
CW9	0.50	3.94	14.54	3.88

Table 8 Continued

No.	t' (ft)	V x 10^{-3} (ft/sec)	τ (lb/ft^2)	ϵ_τ (%)
CW10	0.50	5.36	11.35	6.34
CW11	0.75	0.65	171.29	8.11
CW12	0.75	1.30	93.53	6.79
CW13	0.75	2.64	35.64	4.36
CW14	0.75	3.94	23.79	4.20
CW15	0.75	5.36	16.09	4.18

Note CS: results with small ribs.
CW: results with large ribs.

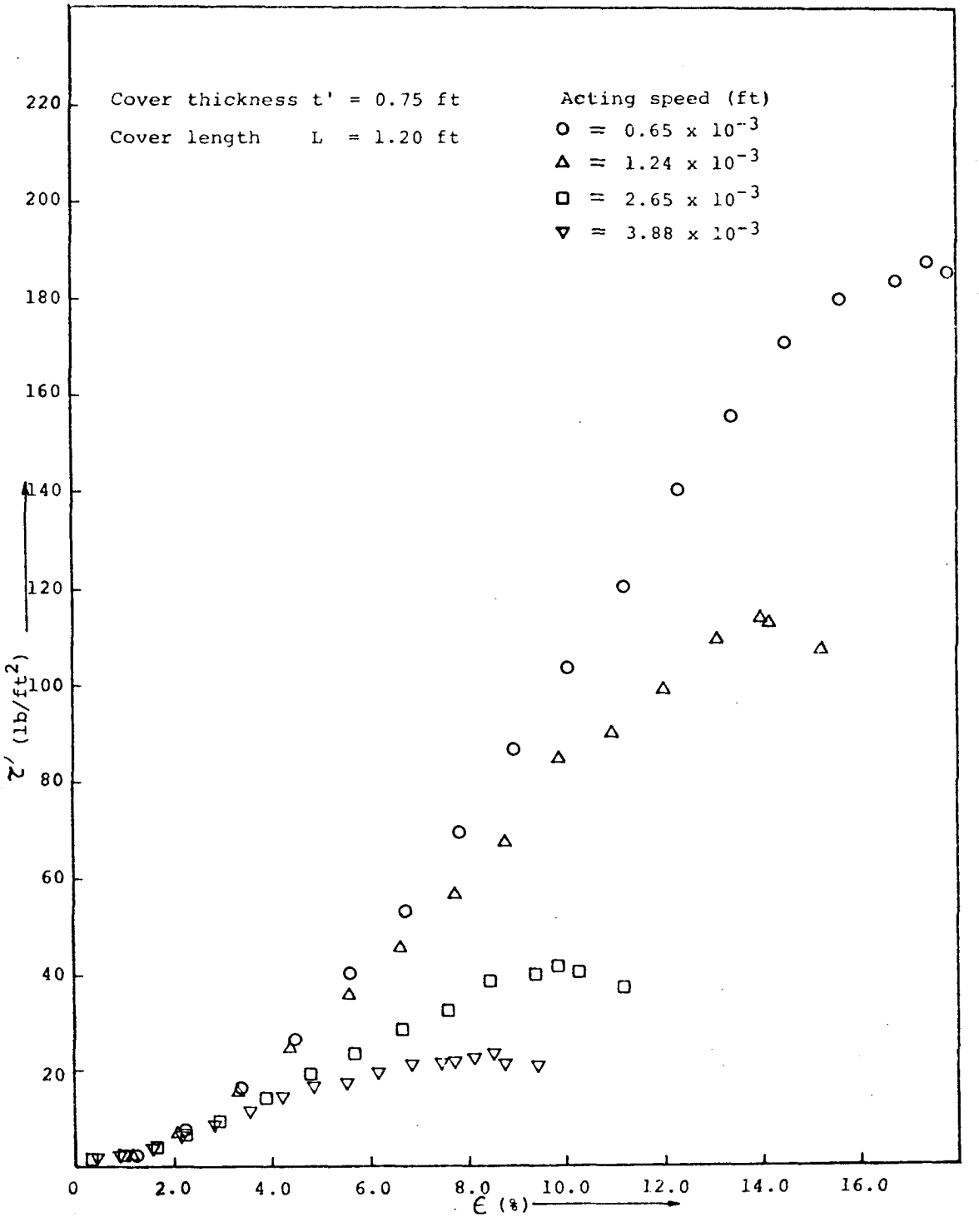

Figure 25. $\tau' - \epsilon$ plots for various acting speed and constant cover thicknesses in rectangular shear apparatus.

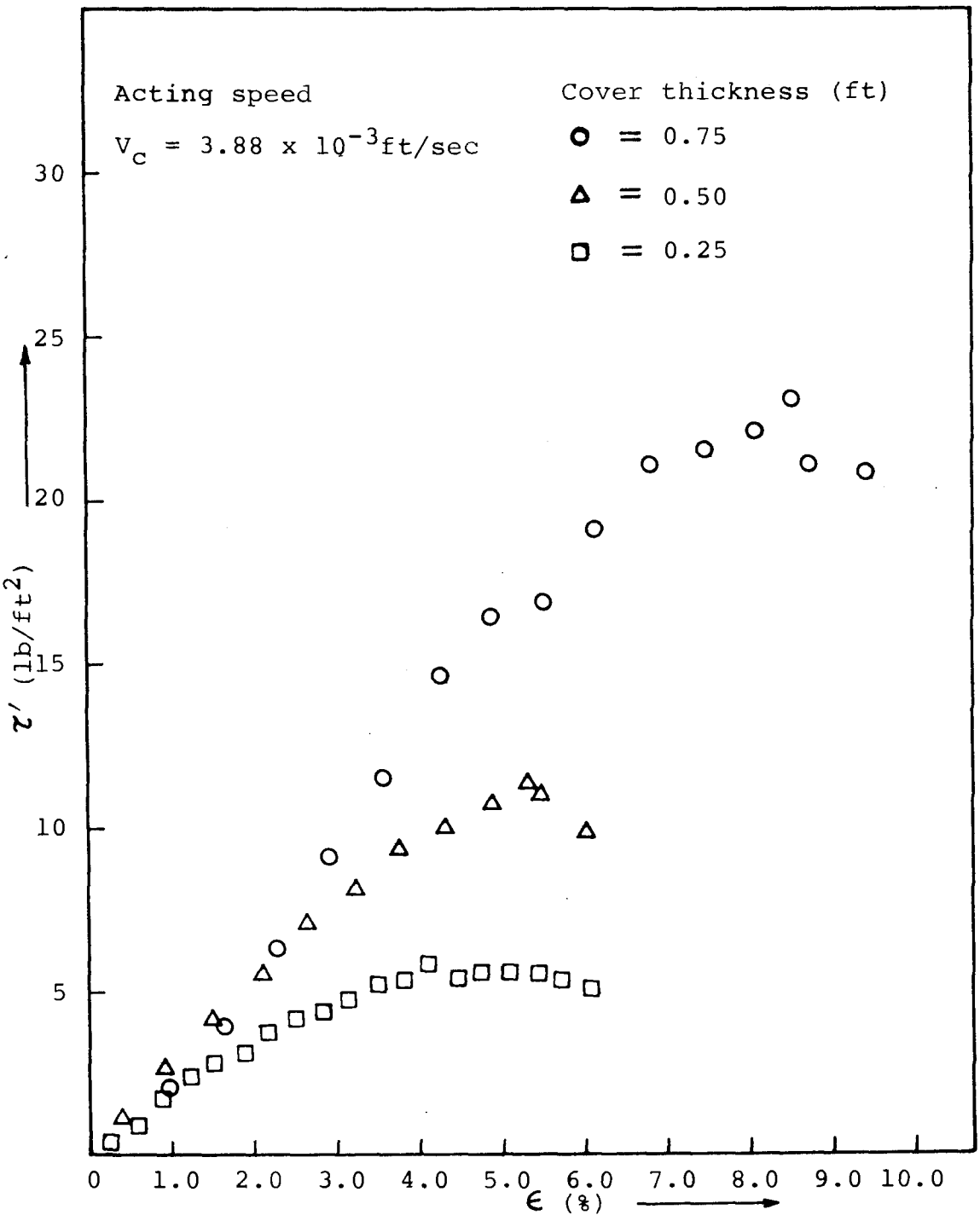

Figure 26. τ' - ϵ plots for various cover thicknesses and constant acting speeds in rectangular shear apparatus.

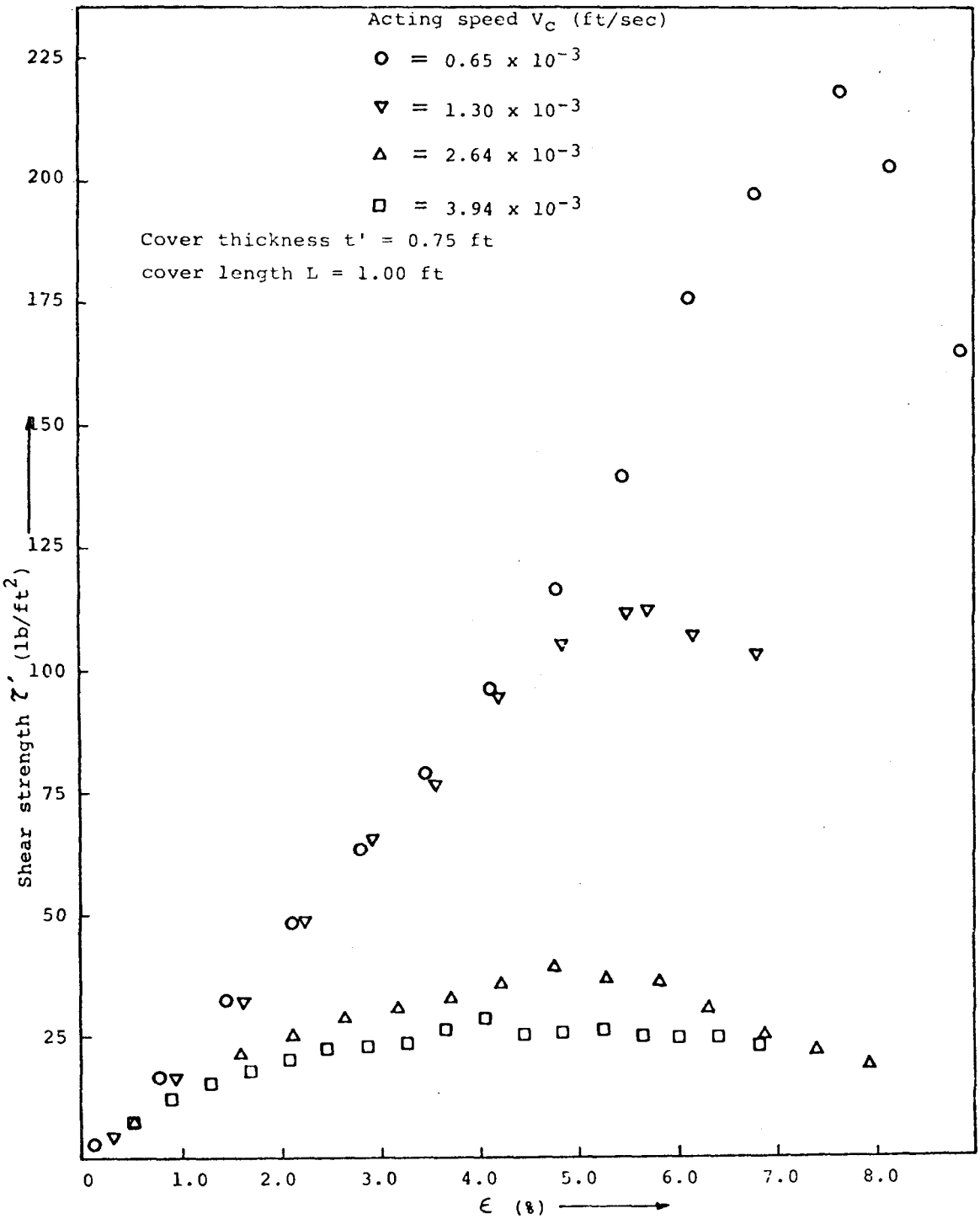

Figure 27. τ' - ϵ plots for various acting speeds and constant cover thicknesses in cylindrical shear apparatus.

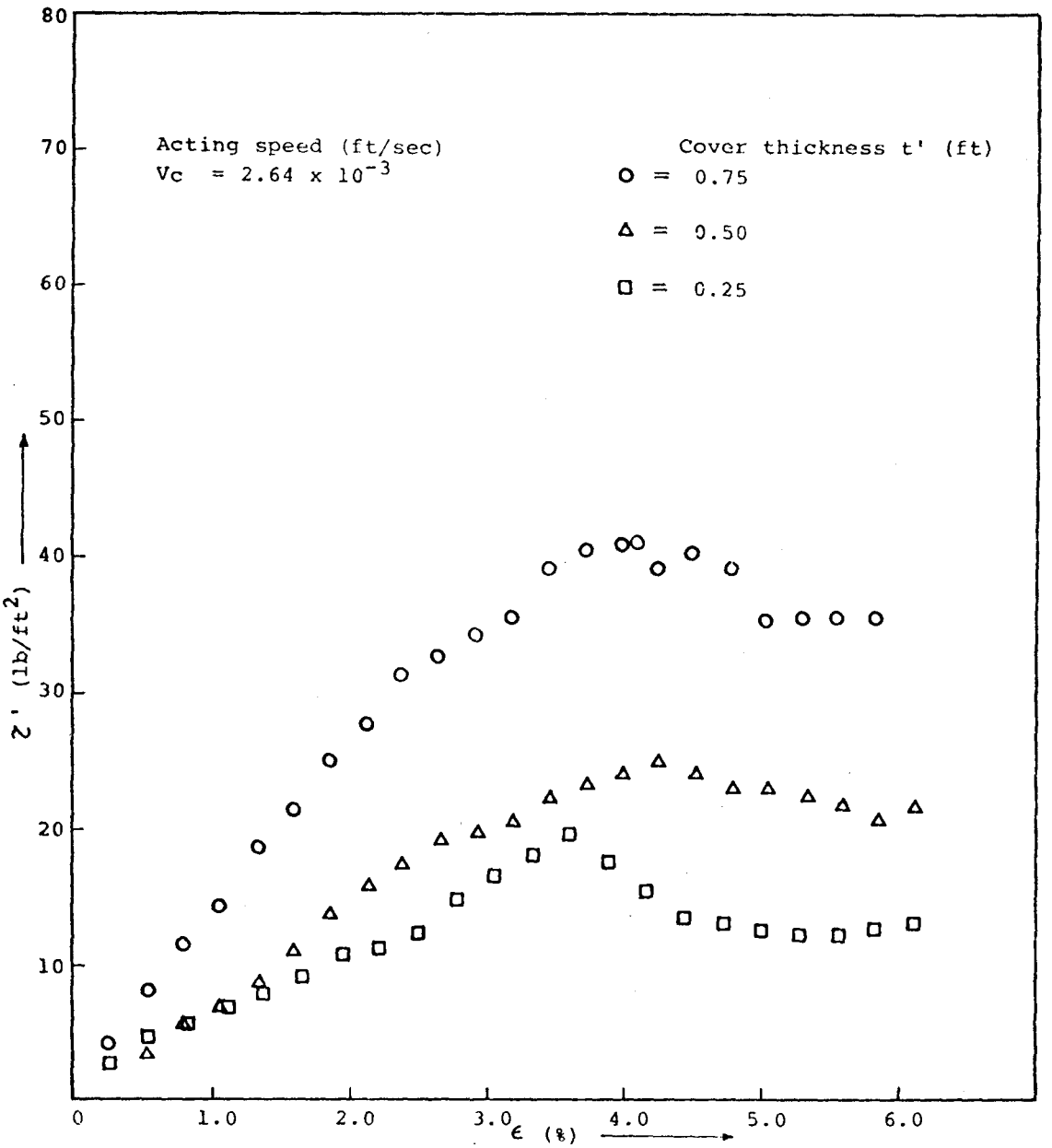

Figure 28. $\tau' - \epsilon$ plots for various cover thicknesses and constant acting speeds in cylindrical shear apparatus.

various ice cover thickness t' are presented in Figures 29 and 30 for the rectangular and cylindrical shear apparatus, respectively. It is seen that in most cases for a given cover thickness, the failure strain decreases nonlinearly with increasing acting speed. This means for the same ice cover thickness, the lower the acting speed the longer the time and the larger the relative displacement ΔL, which are needed for an ice cover to fail under shear. In the tests with rectangular shear apparatus, Figure 29, the failure strain appears to be approximately proportional to cover thickness and length; the effect of the latter being more significant for the larger values of cover thickness. The range of failure strain was found to lie between 18.8% and 3.05% when crushed ice was used.

As seen from Figure 30, the failure strains obtained with the cylindrical apparatus, also decreases with increasing acting speed but no significant effect of the rib sizes could be detected, nor of the cover thickness. The failure strain was found to vary between 8.11% and 2.31%, a range smaller than that obtained with the rectangular shear apparatus.

3. Relation between failure shear strength, acting speed, ice cover thickness and length. From the above presentation, it is known that the acting speed, i.e., deformation rate, cover thickness, and the initial length of the ice cover are the dominant factors influencing the shear strength of ice cover. Plots of the failure shear strength, τ, against the different factors are shown in Figures 31 and 32 for the tests conducted in the rectangular shear apparatus with parallelepiped ice floes and crushed ice, and in Figure 33 for the tests conducted in the cylindrical shear apparatus with crushed ice.

From these figures, it is seen that for constant acting speed the failure shear strength increases linearly with ice cover thickness. The rate of increase of τ with cover thickness decreases with increasing acting speed, V_c, and in fact becomes practically zero for V_c greater than about 0.013 ft/sec. At these large acting speeds, the failure shear strength is approximately equal to 2.0 lb/ft^2, independent of the cover thickness.

Figure 31 presents the results obtained with the rectangular shear apparatus with parallelepiped ice floes. The dotted lines shown

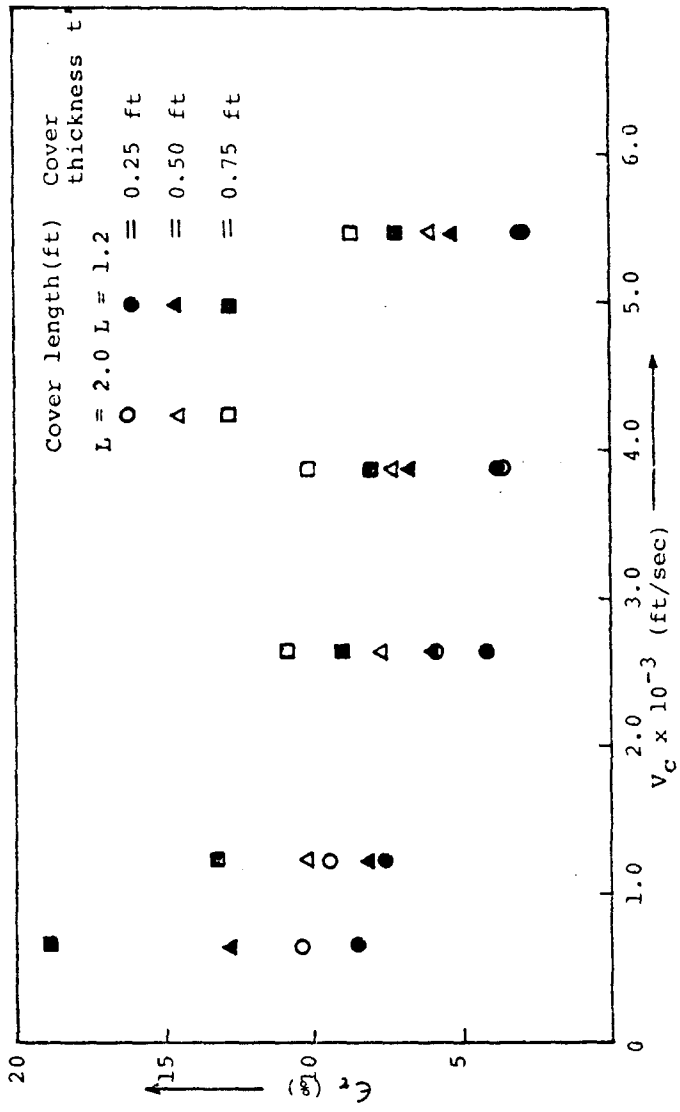

Figure 29. ϵ_τ - V_c diagrams for various ice cover thicknesses and lengths in rectangular shear apparatus. (crushed ice)

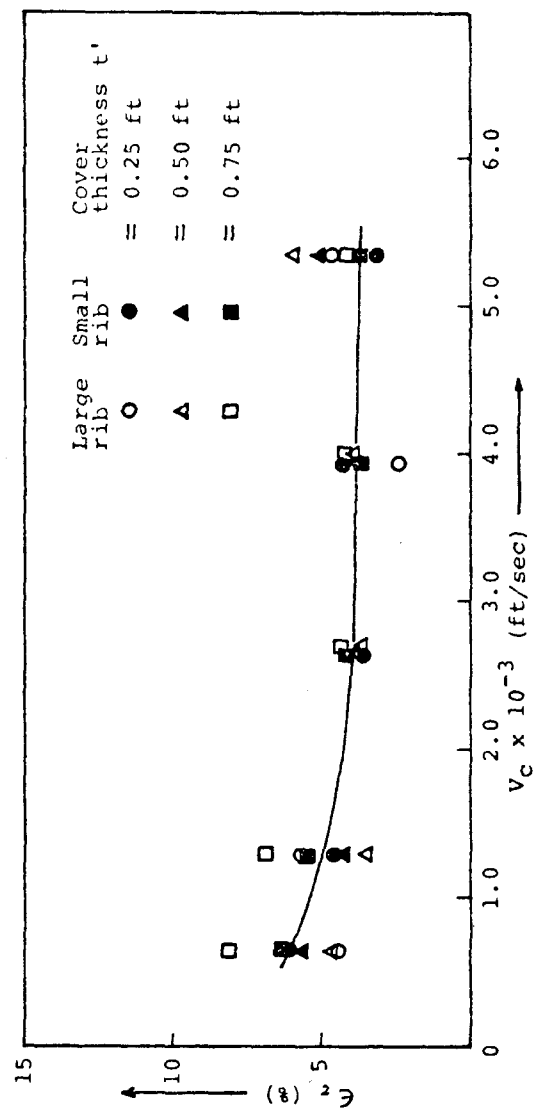

Figure 30. ϵ_z - V_c diagrams for various ice cover thicknesses and lengths in cylindrical shear apparatus. (crushed ice)

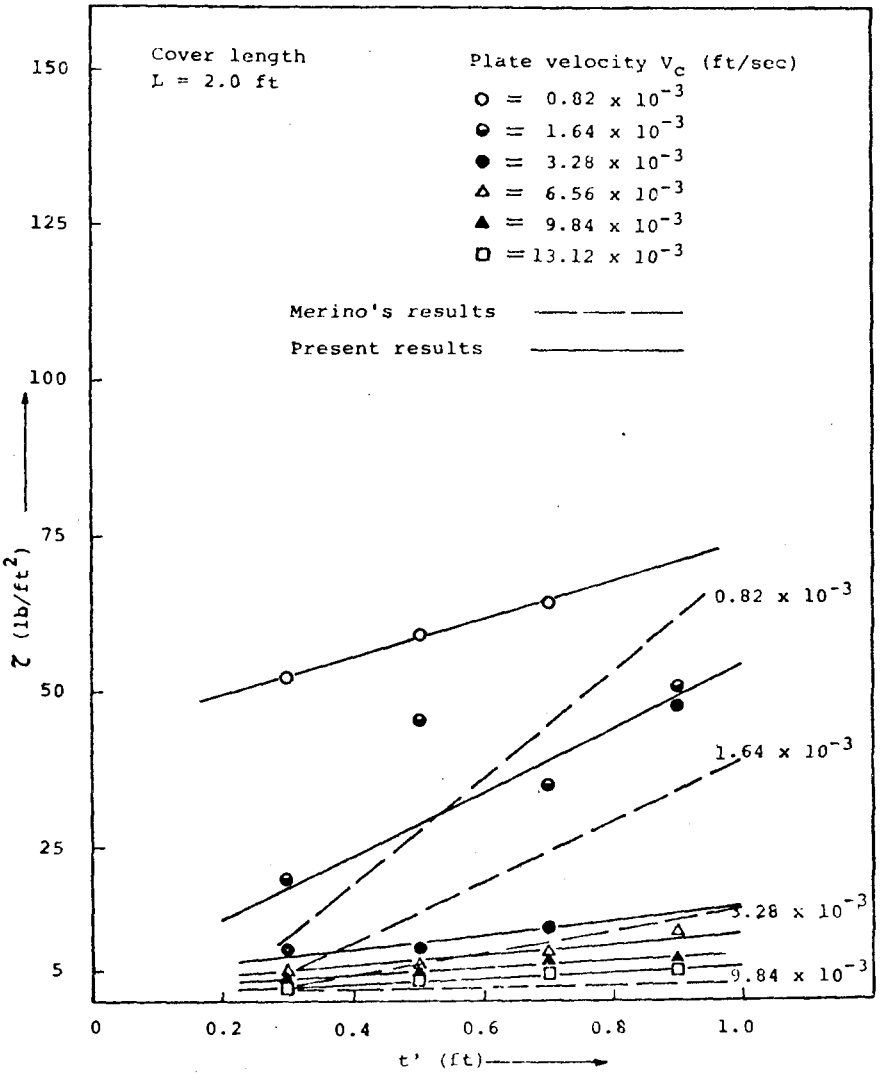

a) L = 2.0 ft

Figure 31. τ - t' plots (rectangular shear apparatus with parallelepiped ice blocks).

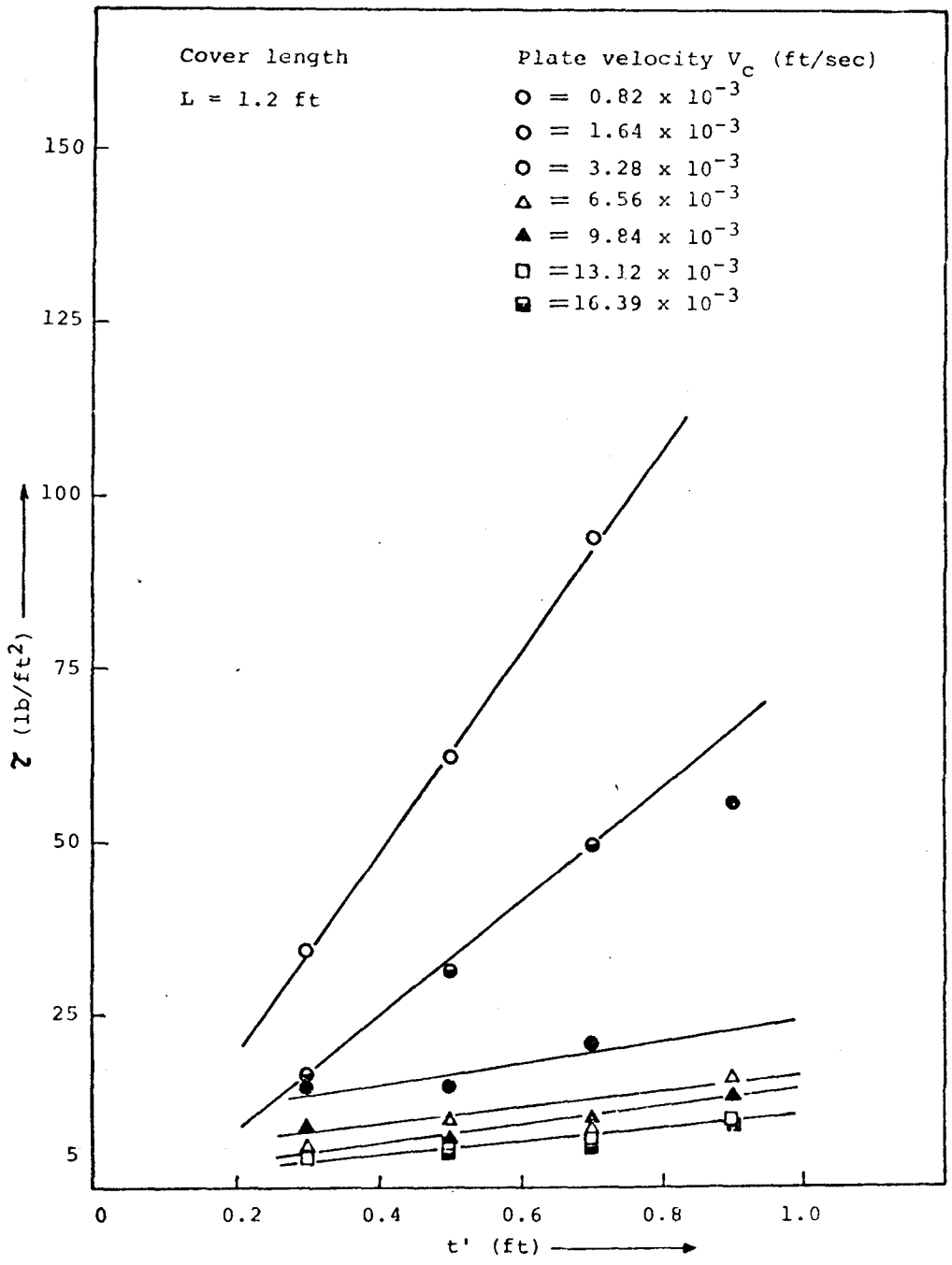

b) L = 1.2 ft

Figure 31. (continued).

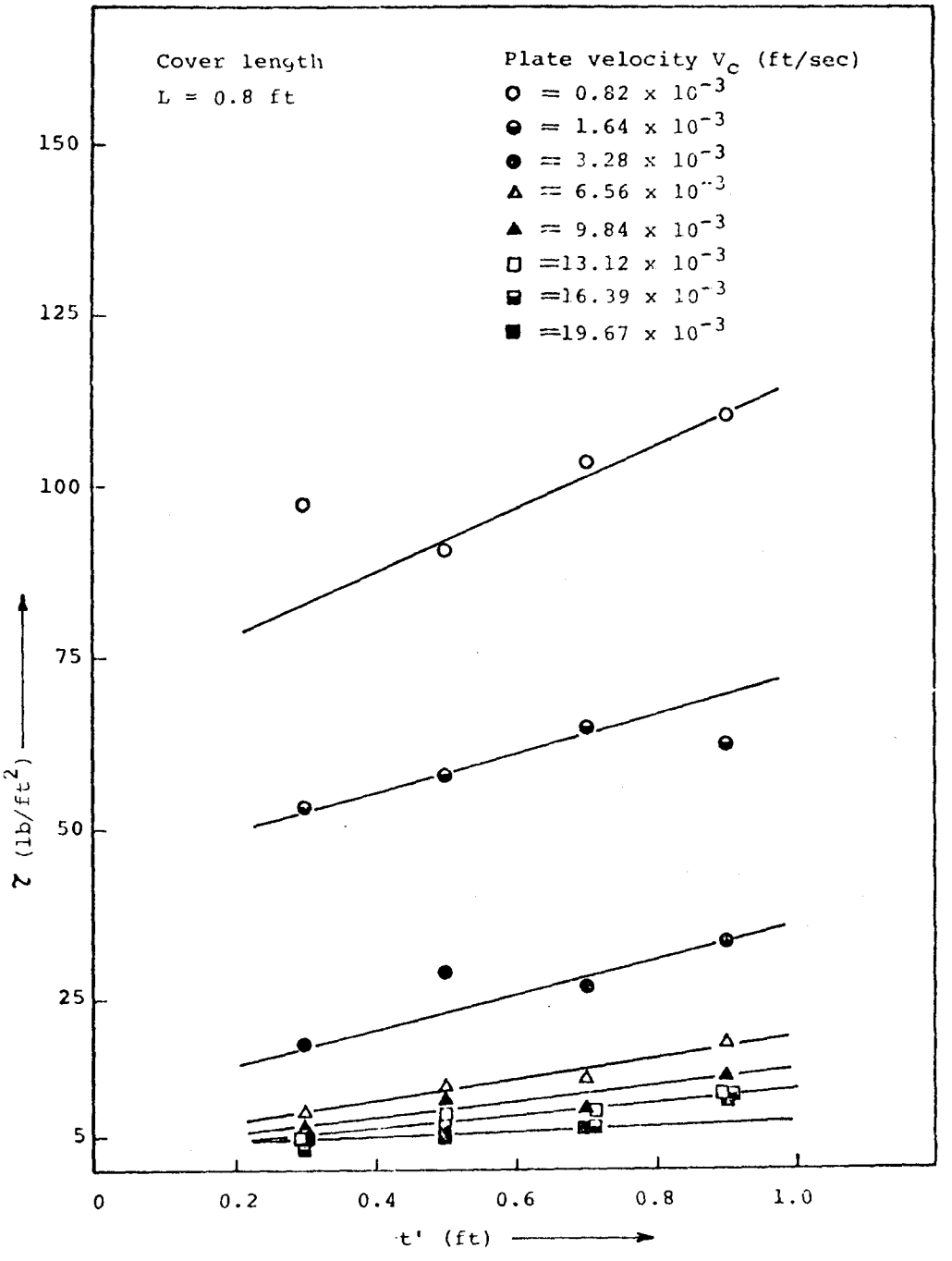

c) L = 0.8 ft

Figure 31. (continued).

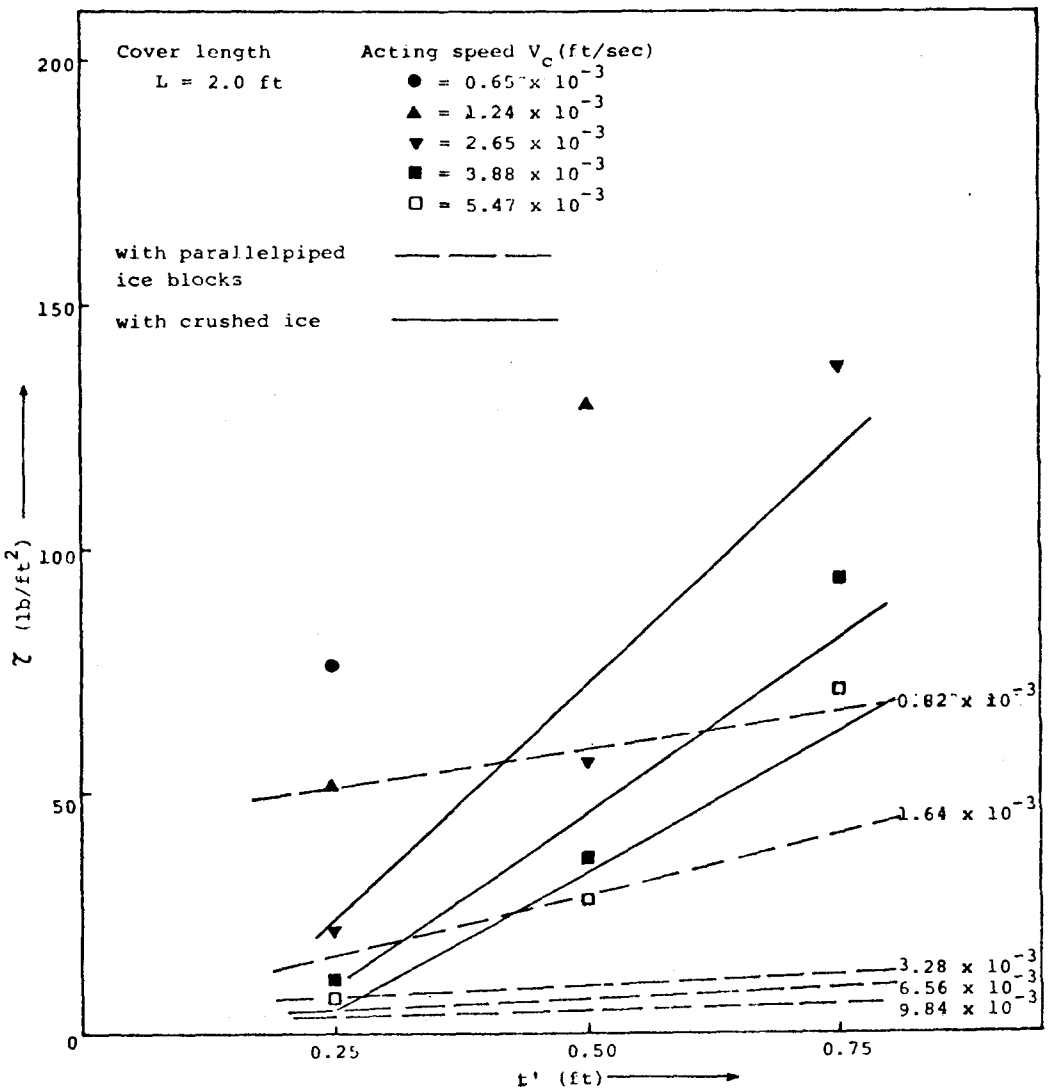

a) L = 2.0 ft

Figure 32. τ - t' plots (rectangular shear apparatus with crushed ice).

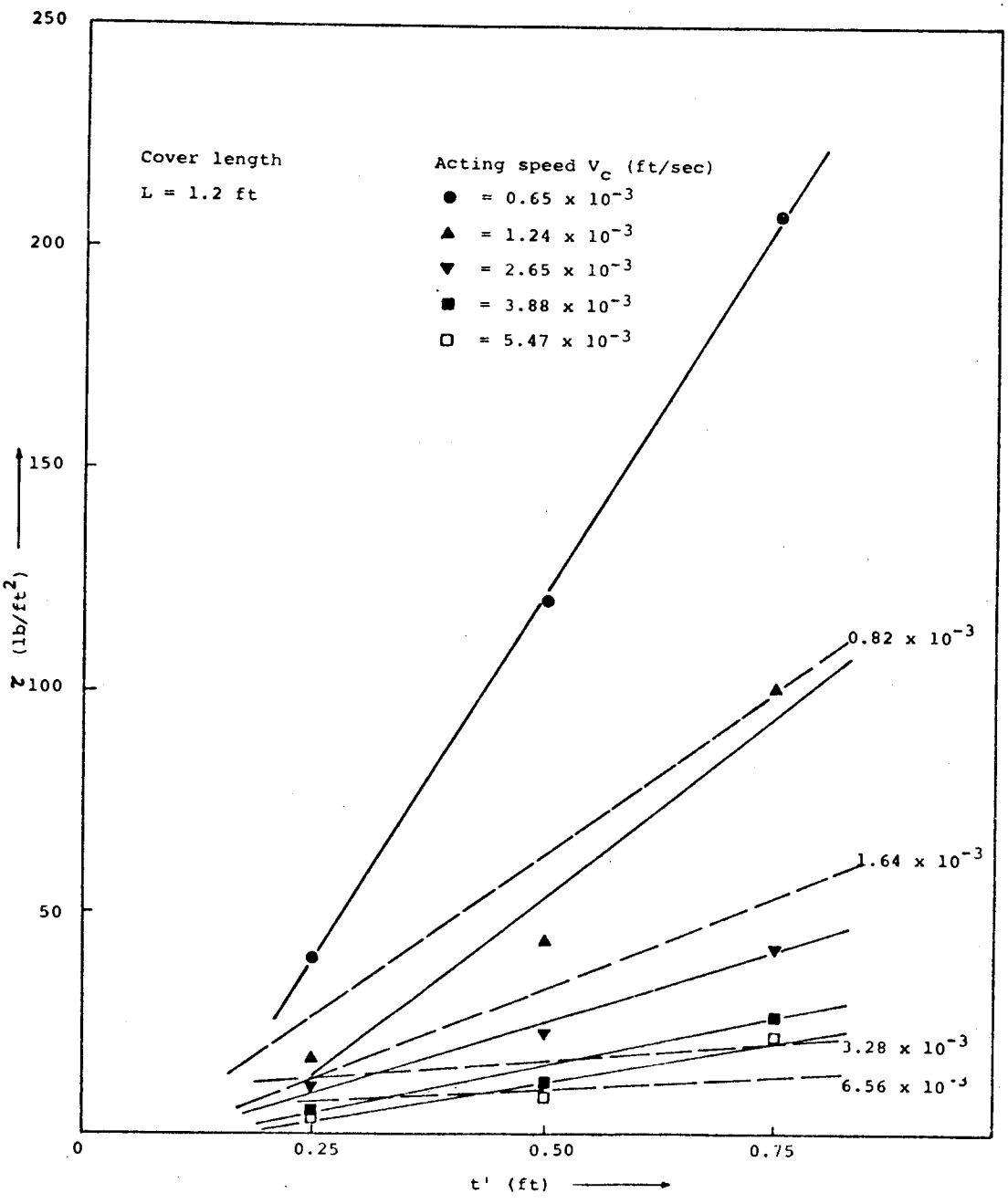

b) L = 1.2 ft

Figure 32. (continued).

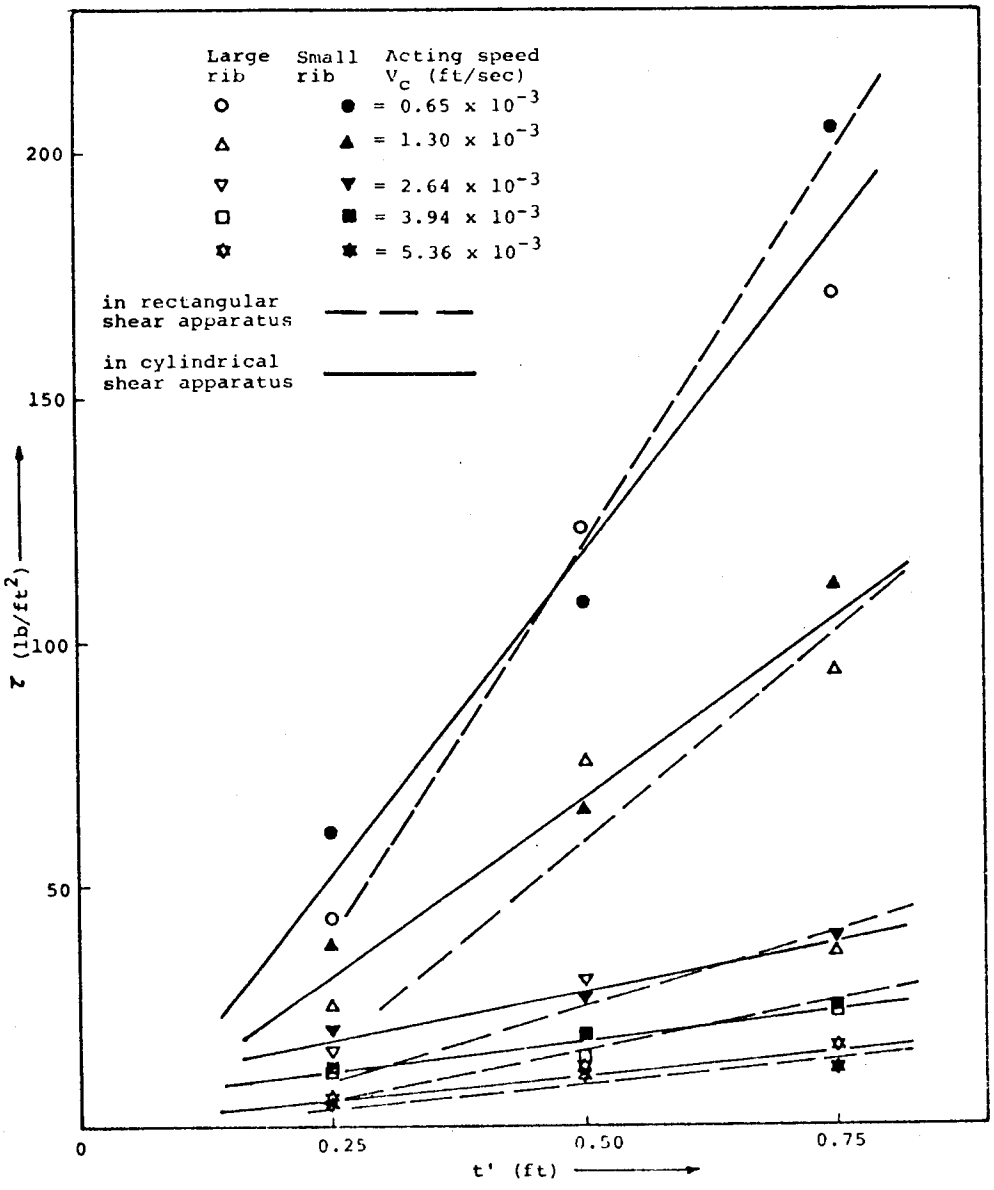

Figure 33. τ - t' plots (cylindrical shear apparatus with crushed ice).

in Figure 31(a) correspond to Merino's (1974) results. The former results are found to be much larger than the latter. This discrepancy confirms that in the original set-up used by Merino a significant part of the shear load was not transmitted to the dynamometer. In addition, the shearing area calculated here taking into consideration the relative displacement, ΔL, was smaller than that used by Merino in his calculation of τ, thus contributing to the higher values of τ found in the present investigation. In Figure 32,which presents the results obtained with crushed ice in the rectangular apparatus, the dotted lines represent the mean results from Figure 31 (ice parallepipeds in rectangular shear apparatus). It is seen that the shear strength of crushed ice is larger than that obtained with ice parallelepipeds. Ice covers made of crushed ice have less proosity, and a larger interparticle contact area. Therefore they can withstand larger shear loads. In Figure 33, results obtained with the cylindrical shear apparatus with either small or large ribs are compared. No significant difference in the values of τ are apparent between these two set-ups. The results agree quite well with each other. This indicates that the size of the ribs on the cylindrical boundary to prevent slippage of the ice along the boundaries of the apparatus did not affect the failure shear strength as long as there is enough space between the cross vanes and outer ribs. The dotted lines in Figure 33 have been taken from Figure 32 with cover length, L, equal to 1.2 ft, for comparison with the results obtained with cylindrical shear apparatus which had an equivalent ice cover length $L = 2\pi R_s$ where R_s is the radius of the shear surface, equal to 1.0 ft. It is apparent that the failure shear strengths measured in either the cylindrical shear apparatus or the modified rectangular shear apparatus are practically identical.

The influence of cover length on the magnitude of the failure shear strength of fragmented ice cover can be inferred by comparing Figures 31 and 32. The results of Figure 32(a) and (b) show that for a given acting speed, the failure shear strength increases with increasing length in agreement with Merino's (1974) findings. On the other hand, the results in Figure 31 show the conflicting phenomenon that failure strength decreases with increasing length. A thorough check of the

experimental procedures for each series of experiments revealed that the results of Figure 31, obtained by Hsu, were arrived at from only one experimental run for each nominal condition, which, as proven by experience, is not enough to establish reliable data on mechanical characteristics of fragmented ice cover. Hence, the results in Figure 31 are doubtful and can not be trusted as indicating the actual trend of τ as a function of cover length. The increase of τ with increasing cover length was explained by Merino (1974) as follows: for a given V, a larger L produces a smaller strain rate; hence a greater time elapses until the shear strength of the ice is reached. This greater time leads to the development of stronger cohesive bonds, and hence increased shear strength.

IV. SUMMARY AND CONCLUSIONS

A. Compression Tests on Fragmented Ice Covers. The compressive strength of fragmented ice covers was investigated by compression tests with and without initial preloading for a range of loading speed V_c and three cover thicknesses. In spite of the large experimental scatter in the results, common to this type of investigation, the following conclusions were reached:

1. The strength σ_{cr} was found to be inversely proportional to the loading speed V_c for $V_c < 0.01$ ft/sec, but to reach a constant value for $V_c > 0.01$ ft/sec.

2. σ_{cr} was an increasing function of the cover thickness t, but, within experimental accuracy, the ratio σ_{cr}/t is approximately independent of t. This ratio σ_{cr}/t was found to vary as V_c^{-1} for low loading speed, but to reach a constant value for $V_c > 0.01$ ft/sec. In the present experiments it was found that

$$\left.\frac{\sigma_{cr}}{t}\right|_{V_c > 0.01} \simeq 10 \text{ lb/ft}^2$$

3. Because of the large discrepancy between the results of the present study and those of a previous similar investigation (Tatinclaux et al., 1976), it was concluded that relatively small variations in the air temperature can have a large effect on the compressive strengths of floating fragmented ice covers. This effect was tentatively attributed to the influence that air temperature probably has on the formation of cohesive bonds between individual particles in a cover.

4. σ_{cr} was found to be virtually unaffected by either the magnitude of the preload, or the type of preload. Differences in σ_{cr} between the results with and without preload were of the same order of magnitude as the experimental accuracy.

The manner in which the preload was applied to the ice cover in this investigation did not, however, correspond to actual field conditions, which in the opinion of the writers would be better approximated by a static preload. Hence, more research should be undertaken on compression tests with static preload. To this end, a new tentative design is suggested and shown in Figure 34. A combination of plate, steel rod, pulley and weight would be used to apply the preload to the ice cover. As shown in Figure 34 false walls would be installed in the force tank, one set across the tank as preloading plate and two longitudinal walls a small distance away from the longitudinal walls of the tank. The preloading plate would be connected by two rods, located in the space between tank and false walls and riding on ball bearings to minimize friction (A-A and B-B sections in Figure 34), to a steel cable passing over a pulley and attached to a hanging weight. This weight would be used as preload and could be changed according to the magnitude of the desired preload. The ice cover would be formed between the plate and force wall. The given static preload would be applied to the ice cover by the hanging weight. After a period of time, the driving plate would be started and the compression test conducted. This design should apply a constant static load to the ice cover and thus the natural condition of preloading would be better simulated.

B. Shearing Tests on Fragmented Ice Covers. The shear strength τ of fragmented ice covers was investigated by direct shear tests with a rectangular apparatus and by vane shear tests with a cylindrical apparatus.

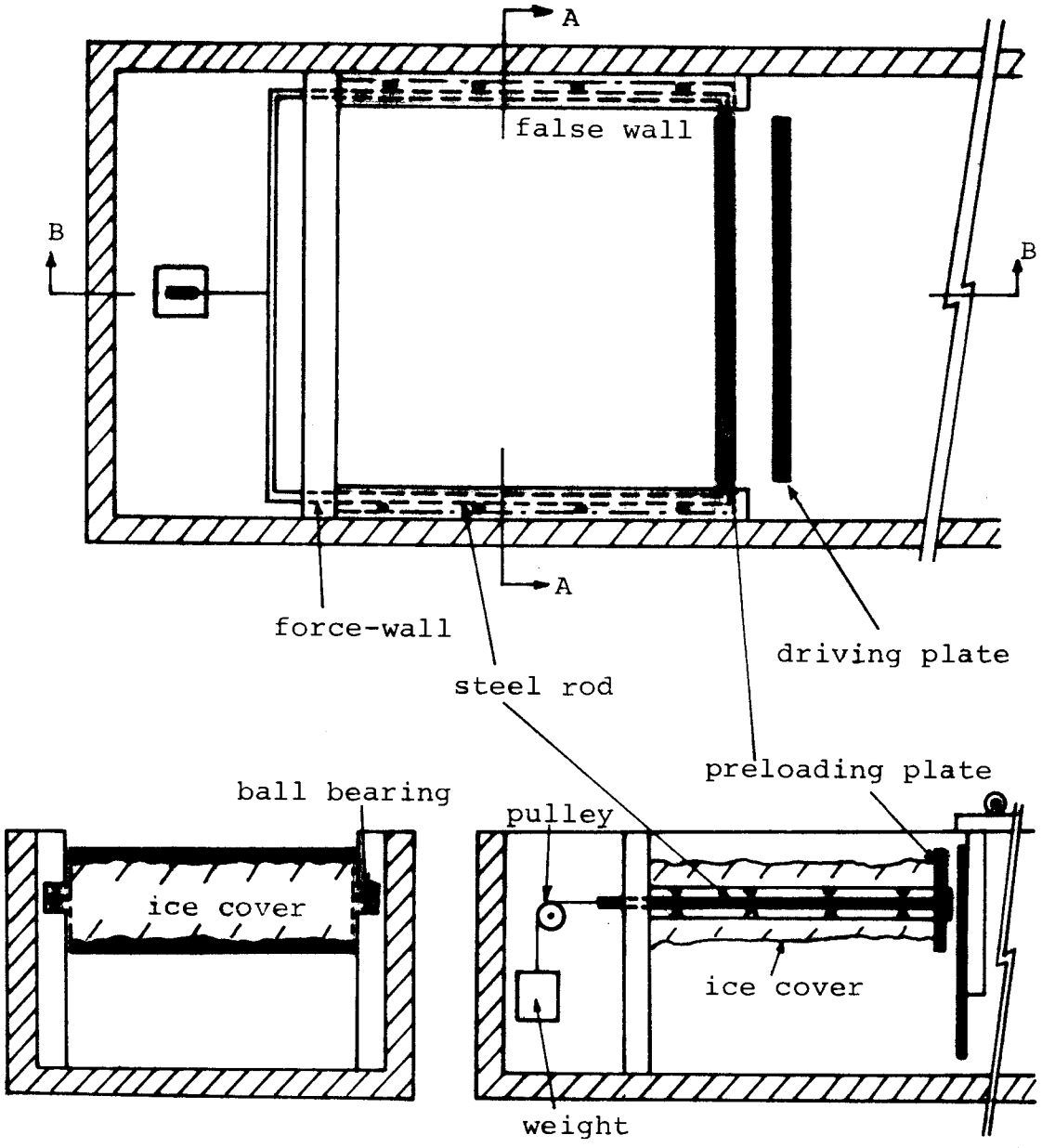

Figure 34. Sketch of proposed apparatus for compression tests with static preloading.

The experiments were conducted for different shearing speed, V_c, ice cover thickness, t, and ice cover length, L. The experimental results can be summarized as follows:

1. τ was found to be inversely proportional to V_c, and proportional to t, as long as V_c was less than 0.01 ft/sec but independent of t and equal to 2.0 lb/ft^2 for values of V_c greater than about 0.01 ft/sec.

2. τ was still found to be affected by cover length in the tests with rectangular shear apparatus. This means that the effects of the compressive stress during shear were not totally eliminated. Furthermore, the influence of L on τ appeared to depend on the configuration of the test apparatus. Further tests using cylindrical shear apparatus of larger dimensions should be undertaken to study the influence caused by the configuration of the test apparatus.

3. τ was found to be affected by the size and shape of the ice samples. Low porosity ice covers made of irregular crushed ice resulted in higher values of τ than when regular shape and parallelepiped ice floes were used to form the fragmented covers.

4. τ was found to be virtually unaffected by either direct shear tests or vane shear tests under nearly same experimental conditions. But, again, more experiments using a larger cylindrical apparatus are needed to verify this conclusion.

REFERENCES

Bolsegna, R.I. (1968) "River Ice Jams", U.S. Army Corps of Engineers, Lake Survey District, Detroit, Research Report 5-5.

Frankenstein, G. and Assur, A. (1972) "Israel River Ice Jam", Intern. Assn. for Hydr. Res., I.A.H.R. Symposium on Ice and its Action on Hydraulic Structures, pp. 153-157.

Merino, M.P. (1974) "Internal Shear Strength of Floating Fragmented Ice Cover", M.S. Thesis, Department of Mechanics and Hydraulics, The University of Iowa, Iowa City, Iowa.

Pariset, E., Hausser, R., and Gagnon, A. (1966) "Formation of Ice Covers and Ice Jams in Rivers", Proc. ASCE, Jour. of Hyd. Div., 92, HY6.

Tatinclaux, J.C., Lee, C.L., Wang, T.P., Nakato, T., and Kennedy, J.F. (1976) "A Laboratory Investigation of the Mechanics and Hydraulics of River Ice Jams", IIHR Report No. 186, Iowa Institute of Hydraulic Research, The University of Iowa, Iowa City, Iowa.

Uzuner, M.S. and Kennedy, J.F. (1974) "Hydraulics and Mechanics of River Ice Jams", IIHR Report No. 161, Iowa Institute of Hydraulic Research, The University of Iowa, Iowa City, Iowa.

U.S. Army Corps of Engineers (1976) "Ice Condition Winter 1965, 1966", U.S. Army Corps of Engineers, Rock Island (Illinois) District, After Action Report.

Unclassified

SECURITY CLASSIFICATION OF THIS PAGE (When Data Entered)

REPORT DOCUMENTATION PAGE

READ INSTRUCTIONS BEFORE COMPLETING FORM

1. REPORT NUMBER: IIHR Report No. 206	2. GOVT ACCESSION NO.
3. RECIPIENT'S CATALOG NUMBER	
4. TITLE (and Subtitle): Compressive and Shear Strengths of Fragmented Ice Covers - A Laboratory Study	5. TYPE OF REPORT & PERIOD COVERED: Final Report, April 1976 - July 1977
6. PERFORMING ORG. REPORT NUMBER: IIHR Report No. 206	
7. AUTHOR(s): S.T. Cheng and J.C. Tatinclaux	8. CONTRACT OR GRANT NUMBER(s): DACA 89-76-G-057
9. PERFORMING ORGANIZATION NAME AND ADDRESS: Iowa Institute of Hydraulic Research, The University of Iowa, Iowa City, Iowa 52242	10. PROGRAM ELEMENT, PROJECT, TASK AREA & WORK UNIT NUMBERS
11. CONTROLLING OFFICE NAME AND ADDRESS: U.S. Army Corps of Engineers, Cold Regions Research and Engineering Lab, Hanover, NH 03755	12. REPORT DATE: August 1977
	13. NUMBER OF PAGES: 82
14. MONITORING AGENCY NAME & ADDRESS (if different from Controlling Office)	15. SECURITY CLASS. (of this report): Unclassified
	15a. DECLASSIFICATION/DOWNGRADING SCHEDULE

16. DISTRIBUTION STATEMENT (of this Report)

Approved for public release; distribution unlimited

17. DISTRIBUTION STATEMENT (of the abstract entered in Block 20, if different from Report)

18. SUPPLEMENTARY NOTES

19. KEY WORDS (Continue on reverse side if necessary and identify by block number)

Compressive Strengths, Experiments, Floating Fragmented Ice Covers, Ice Jams, Shear Strengths

20. ABSTRACT (Continue on reverse side if necessary and identify by block number)

The results of an experimental study on the compressive and shear strengths of floating, fragmented ice covers are presented. The compressive strength of prestrained covers and of covers submitted to an approximately constant preload was found to be essentially equal to that of unstrained, non-preloaded covers. An important finding was that the compressive strength σ_{cr} became independent of the velocity V_c at which the load was applied when V_c became greater than 0.01 ft/sec, and that for $V_c > 0.01$ the ratio of strength to cover thickness t

DD FORM 1 JAN 73 1473 EDITION OF 1 NOV 65 IS OBSOLETE S/N 0102-014-6601 |

Unclassified

SECURITY CLASSIFICATION OF THIS PAGE (When Data Entered)

became, within experimental accuracy, approximately constant independent of both V_c and t. However, the difference observed between the present study and that of a previous, similar investigation led to the conclusion that small variations in the air and/or water temperatures can have a large effect on σ_{cr} and σ_{cr}/t, probably due to their affecting the formation of cohesive bonds between the ice particles within the ice covers.

The shear strength τ of covers of various thicknesses measured in a linear and in a cylindrical apparatus were found to have essentially the same values in both apparatus. The strength τ was found to become independent of both the velocity of application of shear V_c and of the cover thickness for $V_c > 0.01$ ft/sec. The results also showed that the shear strength of covers made of crushed ice was higher than that of covers made of ice parallelepipeds, probably because of the difference in porosity and interparticular surface area between the two types of cover.